JOURNAL OF ENERGY TECHNOLOGY

VOLUME 6 / Issue 4

JOURNAL OF ENERGY TECHNOLOGY

Metanov klatrat – nov energetski vir?

Iz Japonske poročajo, da so marca letos (2013) uspešno pridobili zemeljski plin iz metanovega klatrata z dna oceana. Metanov klatrat poznamo tudi pod imenom metanov led – metan je ujet v zamrznjenih kristalih vode. V svetovnem merilu se ocenjuje, da je zalog metanovega klatrata med 10.500 do 42.000 milijonov kubnih metrov, kar pomeni, da bi zadostilo potrebe po plinu, seveda glede na trenutno porabo, za 3.000 do 12.000 let. To pomeni, da so zaloge metanovega klatrata vsaj dvakrat tolikšne kot vse svetovne zaloge premoga, nafte in naravnega plina skupaj. Nahajališča ležijo pod vodo večinoma na mejah kontinentalnih plošč. V primeru ležišča na robu strmo padajočega roba kontinentalne plošče, bi lahko bilo nepremišljeno odstranjevanje metanovega klatrata nevarno. Sprožil bi se namreč lahko podvodni plaz peščenih plasti v večje globine, kar pa bi lahko na površini vode ustvarilo močne cunamije.

Japonska vrtalna ladja je v Nankajski udorini, južno od Tokia, testno načrpala 120.000 kubičnih metrov zemeljskega plina. Vrtina poteka skozi 1.000 m morske vode, ter skozi 270 m morskih usedlin (v glavnem so to peščene usedline). Pod temi usedlinami leži 60 m debela plast metanovega klatrata. Črpanje poteka tako, da se voda izčrpava iz plasti metanovega klatrata, s čimer se zniža tlak vode in omogoči odtajanje ledu, ki tako omogoča sproščanje metana v plinasti obliki. Vrtalno/transportna cev je dvoslojna, oz. kolobarjaste oblike. Notranja cev je uporabljena za črpanje vode, med zunanjim obodom notranje cevi in notranjim obodom zunanje cevi, pa se omogoča črpanje metana. Druga možnost sproščanja metana bi bila s segrevanjem plasti metanovega klatrata, kar pa bi bilo energetsko gledano precej bolj potratno.

Tehnološko gledano je potrebno črpanje in sam transport plina še izpopolniti. Pri črpanju se namreč pojavljajo problemi zamašitve črpalk, v katere zaide pesek. Pri transportu plina sta možni dve izvedbi, in sicer skladiščenje in utekočinjanje plina na plavajoči platformi ob samem črpališču, ali izgradnja plinovoda po ceveh, nameščenih po morskem dnu. Slednja je seveda precej dražja rešitev od prve; ima pa to prednost, da bi se lahko ploščad »selila« od nahajališča do nahajališča.

Ocena zalog v Nankajski udorini je dobrih sedem milijonov kubičnih metrov zemeljskega plina – metana, kar pomeni, da bi Japonska samo s tem virom lahko zadovoljila svoje potrebe po energentih za naslednjih 100 let. Podatki so povzeti po »Nov Vir Energije, Science Illustrated, november 2013«.

Krško, november 2013

Andrej PREDIN

Methane clathrate – a new energy source ?

In March 2013, it was reported that natural gas from methane clathrate had been successfully obtained from the bottom of the ocean near Japan. Methane clathrate (also known as ice methane) is methane trapped in crystals of frozen water. Globally, it is estimated that the world's sources of methane clathrate are between 10,500 to 42,000 million cubic meters, which means that it could cover the world's needs for gas (calculated according to current consumption) for 3,000 to 12,000 years. This means that the stock of methane clathrate is at least twice that of the world's combined coal, oil and natural gas stocks. Deposits lie under water, mostly at the limits of the continental plates. Pumping at the plate edge could be dangerous, possibly triggering underwater avalanches of sand layers at substantial depths, which could create powerful tsunamis on the water surface.

A Japanese drill ship in the Nankai depression, south of Tokyo, test extracted 120,000 cubic meters of natural gas, boring through 1,000 meters of sea water, and through 270 m of mostly sandy sediment. Under these deposits is a 60-m thick layer of methane clathrate. Pumping is carried out so that the water is depleted from the layer of methane clathrate, thereby reducing the water pressure and allowing the ice to defrost, thus allowing the release of methane in the gaseous form. The drilling/conveying pipe layer has an annular shape. The inner pipe is used for the pumping of water, while methane is extracted via the outer periphery of the inner tube and the inner circumference of the outer tube. Alternatively, the release of methane would be by heating the layer of methane clathrate, which would be much more wasteful with regard to energy usage.

Technologically speaking, there must be improved absorption and transport of gas itself. When pumping, some problems exist with the clogging of pumps with sand. When transporting gas, two possibilities exist: storage and liquefaction of gas on a floating platform next to the pumping station, or the construction of a pipeline installed on the seabed. The latter is, of course, a much more expensive solution than the former, but the former has the advantage that the platform can be moved from deposit to deposit.

It is estimated that the Nankai depression holds more than seven million cubic meters of natural gas (i.e. methane), which means that it is the only source capable of meeting Japan's energy demand for the next 100 years. This information is taken from the "New Source of Energy, Science Illustrated", November 2013.

Krško, November, 2013

Andrej PREDIN

Table of Contents /
Kazalo

OPTIMIZATION METHOD FOR CONTROL OF VOLTAGE LEVEL AND ACTIVE POWER LOSSES BASED ON OPTIMAL DISTRIBUTED GENERATION PLACEMENT USING ARTIFICIAL NEURAL NETWORKS AND GENETIC ALGORITHMS

OPTIMIZACIJSKA METODA ZA NADZOR NAPETOSTNIH NIVOJEV IN IZGUB Z UPOŠTEVANJEM OPTIMALNE IMPLEMENTACIJE RAZPRŠENE PROIZVODNJE S POMOČJO NEVRONSKIH MREŽ IN GENETSKIH ALGORITMOV

Marko Vukobratović[ℜ], Predrag Marić, Željko Hederić

Abstract

This paper presents a method for reducing active power system losses and voltage level regulation by implementing adequate distributed generation capacity on the appropriate terminal in a distribution system. Active power losses are determined using an Artificial Neural Network (ANN) using simultaneous formulation for the determination process based on voltage level control and injected power. Adequate installed power of distributed generation and the appropriate terminal for distributed generation utilization are selected by means of a genetic

---

ℜ Corresponding author: Marko Vukobratović, Tel.: +385 31 224 656, Fax: +385 31 224 605, Mailing address: vukobratovic@etfos.hr

----

algorithm (GA), performed in a distinct manner that fits the type of decision-making assignment. The training data for Artificial Neural Network (ANN) is obtained by means of load flow simulation performed in DIgSILENT PowerFactory software on a part of the Croatian distribution network. The active power losses and voltage conditions are simulated for various operation scenarios in which the back propagation artificial neural network model has been tested to predict the power losses and voltage levels for each system terminal, and GA is used to determine the optimal terminal for distributed generation placement.

<u>Povzetek</u>

V članku je predstavljena metoda za zmanjšanje izgub v sistemu in regulacijo napetostnih nivojev z implementacijo razpršenih proizvodnih kapacitet na primernih terminalih distribucijskega sistema. Izgube delovne moči so določene z uporabo Umetne Nevronske Mreže (UNM), kjer je uporabljena sočasna formulacija v procesu odločanja na osnovi nadzora napetostnih nivojev in injiciranih moči. Ustrezne inštalirane moči razpršene proizvodnje in primerni terminali za izkoriščanje razpršene proizvodnje so izbrani na osnovi Genetskih Algoritmov (GA) izvedenih na poseben način, ki ustreza nalogam v procesu odločanja. Podatki za Umetno Nevronsko Mrežo so pridobljeni na osnovi simulacije pretoka energij v programskem paketu ''DIgSILENT PowerFactory'' na delu Hrvaškega distibucijskega omrežja. Simulacije izgub delovne moči in napetostnih razmer so izvedene za različne obratovalne scenarije, v katerih je testiran model ''vzratnega učenja'' umetne nevronske mreže za predvidevanje izgub moči in napetostnih nivojev za vsak sistemski terminal. Genetski algoritem je uporabljen za določitev optimalnega terminala za umestitev razpršene proizvodnje.

1   INTRODUCTION

The presence of distributed generation (DG) changes the load characteristics of the distribution network, which gradually becomes an active load network and implies changes in the power flow. Current-voltage conditions are now not only dependent on the current consumption but also on the production from DG. If sized and selected properly, DG can improve electrical conditions, such as improvement of voltage, loss reduction, relieved transmission and distribution congestion, improved utility system reliability and power quality in the distribution network, [1].

In order to determine the impact on the power system of each DG, it is necessary to perform the power flow analysis on a daily or hourly (or even 10-minute) basis. Due to the increased number of small DG, mostly from intermittent sources, it is necessary to implement an advanced management power distribution system to make the distribution network significantly automated. Accordingly, it is necessary to develop mathematical optimization models that can be implemented in the distribution network management system to enable optimal management. According to [2], an automated distribution network has to provide a fast and the accurate solution for power flow and current-voltage conditions control.

As an ideal solution, artificial neural networks (ANN) are imposed due to their ability to solve nonlinear problems in a short period of time, and if quality organized and made, they are able to perform real-time calculations necessary for the optimization of the distribution network. ANN have considerable potential in control systems because they can learn and adapt, they can approximate nonlinear functions, they are suited for parallel and distributed processing and model multivariable systems naturally, [3]. Since they are based on human experience and on

Optimization method for control of voltage level and active power losses based
on optimal distributed generation placement using Artificial Neural Networks
and Genetic Algorithms

----

logical links between inputs and outputs, they can adopt various learning mechanisms and self-organization or training concepts, pattern recognition, forecasting etc.

ANN can be trained to generate control parameters for minimizing power losses and determining the optimal solution for DG implementation in the distribution network. This paper proposes an online real-time power flow optimization and voltage regulation method using ANN and a Genetic Algorithm (GA). ANN are highly robust and provide satisfactory solutions if provided with quality data and can dynamically determine the most appropriate DG solution by means of installed power and position in the system. The GA is used for solving constrained and constrained optimization problems and is based on a natural selection process that mimics biological evolution. The algorithm generates a population of individual solutions that are randomly selected from the population and used as parents for the next generation. Over several generations, the optimal population solution appears.

2   THE PROBLEM FORMULATION

Optimization problem can be generally shown with a model of the objective function and associated restrictions:

$Min f(x,u)$

So that

$$g(x,u) = 0 \tag{2.1}$$

$$h(x,u) \leq 0$$

Where vector **u** is a vector of control variables, **x** is a vector of state variables; scalar f(x) is the objective function, while restrictions are given by the system of equation g(x, u) and inequalities h(x,u).

The main goal of the proposed method is to determine the best locations in the distributed system for distributed generation by minimizing different functions related to project goals which are:

1.   Reduction of active power losses

2.   Voltage profile improvement

2.1   Objective function

The main objective function could be described as:

$$F = Min P_{losses} \tag{2.2}$$

Where P_{losses} are losses of active power in a system.

Minimization of active power losses is an essential requirement in a distribution system for efficient power system operation, [3]. Power losses can be calculated as:

$$P_{losses} = \sum_{i=1}^{N_B} \sum_{j=1}^{N_B} A_{ij}\left(P_i P_j + Q_i Q_j\right) + B_{ij}\left(Q_i P_j + P_i Q_j\right)$$

(2.3)

Where:

P, Q : real power and reactive power injection at respected terminal

N_B : terminal number

And $A_{i,j}$ $B_{i,j}$ are represented respectively:

$$B_{ij} = \frac{R_{ij}\sin(\delta_i - \delta_j)}{V_i V_j}, \quad A_{ij} = \frac{R_{ij}\cos(\delta_i - \delta_j)}{V_i V_j}$$

(2.4)

R_{ij} : line resistance between terminal i and terminal j

V, δ : voltage and load angle at the selected terminal

2.2   Constraints

The objective function of active power loss minimization is not sufficiently suitable without technical restrictions and correct formulation of optimization constraints. Optimal placement of distributed generation and the solution provided with the proposed method must be realistic and should not produce negative impacts on other system aspects. In order to achieve this goal, operational constraints should be properly evaluated and chosen, not only to enable proper operation of the proposed algorithm, but also to support the regular operation of the power system.

2.2.1 Power constraints

For the safe operation of the power system, the active power constraints are given by the expression:

$$P_{Gi} - P_{ti} - V_i \sum_{j=1}^{n} V_j \cdot \left(G_{ij}\sin(\theta_{ij}) + B_{ij}\sin(\theta_{ij})\right)$$

(2.5)

Where:

$i \in n$: number of nodes in network

P_{Gi} : active power production in node i

P_{ti} : active power consumption in node i

θ_{ij} : angle of mutual admittance $\overline{Y_{ij}}$ of nodes i and j

G_{ij} : mutual conductance of nodes i and j

Optimization method for control of voltage level and active power losses based
on optimal distributed generation placement using Artificial Neural Networks
and Genetic Algorithms

B_{ij} : mutual susceptance of nodes i and j

G_{ii} : self-conductance of node i

B_{ii} : self-susceptance of node i

Reactive power restrictions are given by the expression:

$$Q_{Gi} - Q_{ti} - V_i \sum_{j=1}^{n} V_j \cdot \left(G_{ij} \sin(\theta_{ij}) + B_{ij} \sin(\theta_{ij}) \right) \tag{2.6}$$

Where:

$i \in n$: number of nodes in network

Q_{Gi} : reactive power production in node i

Q_{ti} : reactive power consumption in node i

Besides active and reactive power constraints, the apparent power that is transmitted through each branch has to be below the physical limit of the branch transformer in steady-state operation. The constraint of apparent power is given by:

$$S_i \leq S_{i,\max} \tag{2.7}$$

Where:

S_i : apparent power in i[th] branch

$S_{i,\max}$: maximum allowed apparent power in i[th] branch

2.2.2 Voltage levels constraints

Voltage level restrictions are given by the expression:

$$V_{i-\min} \leq V_i \leq V_{i-\max} \tag{2.8}$$

Where:

$i \in n$: number of nodes in network

$V_{i-\min}, V_{i-\max}$: voltage limitations

V_i : voltage level in node i

2.2.3 Constraints of reactive power production in generator node

The generator has the capability curve and the technical operational limits, so the reactive power production is given by the expression:

$$Q_{Gi-\min} \le Q_{Gi} \le Q_{Gi-\max} \quad i \in \{N_{pv}, N_0\}$$ (2.9)

Where:

$Q_{Gi-\min}, Q_{Gi-\max}$: reactive power production limits in node i

N_{pv} : number of PV node

N_0 : node of DG

The objective function including the reduction of active power losses only could provide the solution without predicting a sufficient amount of reactive power reserves in case of the failure of one or more components in a power system. The appropriate optimization solution has to provide the optimization of voltage levels, voltage reduction, loss of stability risk and the reduction of power losses.

3   ARTIFICIAL NEURAL NETWORK DESIGN AND IMPLEMENTATION

Bearing in mind all restrictions and the objective of the optimization, a useful algorithm has to be developed. Because of the complexity and nonlinear interdependence of controlled variables, it is difficult to provide a fast and correct solution using classic (exact) optimization techniques, such as linear programming, the interior point method or mixed integer programming, [5]. ANN can be appropriate for solving such non-linear problems. There are several different types of ANN, including feed-forward neural network, radial basis function (RBF) network, Kohonen self-organizing network, recurrent neural network (RNN), bi-directional RNN, stochastic neural networks, etc. The appropriate neural network has to be properly selected since not every type of neural network will give the best solution for a certain problem. Back-propagation (BP) ANN can be used for the optimization problems since it meets the specific criteria: a flow chart of the problem can be described; there is a relatively easy way to generate a significant or at least necessary number of input and output examples; the problem appears to have considerable complexity but there is a clear solution; outputs may be unambiguous in some extreme cases.

The typical back-propagation network has an input layer, an output layer, and at least one hidden layer. The numbers of hidden layers are theoretically infinite but usually one to four layers is adequate to solve any kind of complex problems.

Each layer has to be fully connected to the vicinal layer by every neuron, as shown in Figure 1.

The relationship between input and output values of multi-layer ANN can be represented as [6]:

$$y = f\left(\sum_{i=0}^{N-1} W_i \cdot X_i(t) - k\right)$$ (3.1)

Where:

y : output value

Optimization method for control of voltage level and active power losses based
on optimal distributed generation placement using Artificial Neural Networks
and Genetic Algorithms

X_i : input value

W_i : weighting factor

k : threshold value

N : layer number

f : nonlinear function

When the network is created, the process of teaching has to be done in order to organize the neurons. This teaching makes usage of a learning rule, which is the variant of the Delta Rule, [3] The teaching starts with determining the error, which is the difference between the actual outputs and the desired outputs given in the training data. Based on this error, the weighting factor is changed in proportion to the error for the global accuracy. The algorithm for the weighting factor changing based on training data is, [6]:

$$\Delta_p W_{ji} = n(t_{pj} - o_{pj})i_{pi} = n\delta_{pj}\, i_{pi} \tag{3.2}$$

Where:

n : learning rate

t_{pj} : j component of pth target output

o_{pj} : j component of pth computed output

i_{pi} : i component of pth input pattern

δ_{pj} : error of target and computed output

If well trained, an ANN can provide reasonable outputs for a new set of inputs enabling network training on a representative set of inputs with output correction. The training should be done on the largest possible set. Generally, the precision of ANN is increased by the larger training set with more input variables.
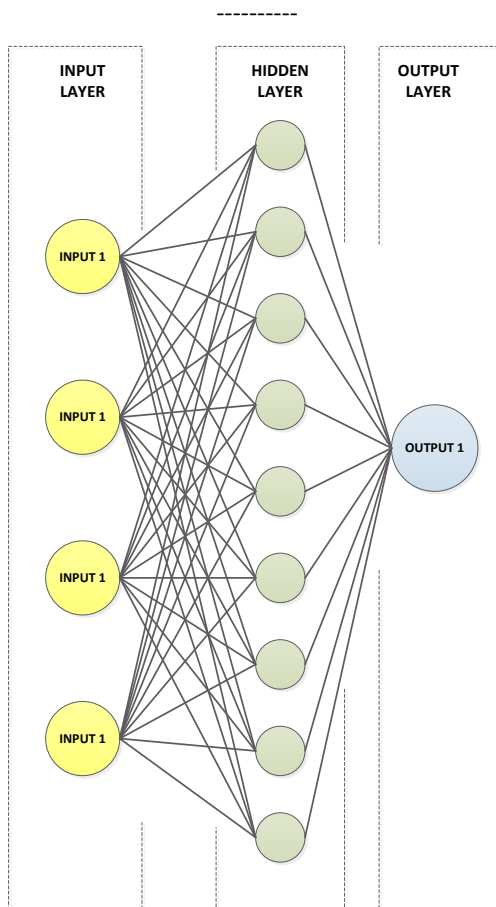
Figure 1: *Structure of Artificial Neural Network*

3.1   Neural network training

For the purpose of ANN training, a training data set has to be generated. Selecting the amount and type of training data is extremely important since the wrong selection could reduce the learning ability of the ANN or even provide an incorrect solution. For better accuracy, all dependent parameters have to be taken into account. The training data for the ANN consists of: DG active power production changed by operation scenarios from 0 kW (no production) to 1.350kW (excessive production) in 10kW increments, injected current from DG production given in kA, and the voltage level on the low-voltage side and the voltage level on the medium-voltage side, given in per-unit (p.u.) values. Targeted data for the ANN training are total feeder losses for each operation scenario. Accordingly, ANN has four input units and one output unit connected with nine hidden layer units.

The training is performed by the Levenberg-Marquardt algorithm for nonlinear least square problems, [7]. Calculations of each operation scenario for the training data generation are performed using DIgSILENT PowerFactory software, a leading power system analysis tool for applications in generation, transmission, distribution and industrial systems, [8]. The ANN is first trained on sample values for one terminal, and later it is tested on all proposed terminals.

Optimization method for control of voltage level and active power losses based
on optimal distributed generation placement using Artificial Neural Networks
and Genetic Algorithms

The results of each operation scenario are introduced into tables. The power losses in the electrical network can be computed by means of load flow simulation generated in the DIgSILENT PowerFactory software. Quantification and determination of power losses is essential due to the impact on the power system economic operation and the lifetime of the included equipment, [9]. Performance of ANN training is shown in Figure 2.
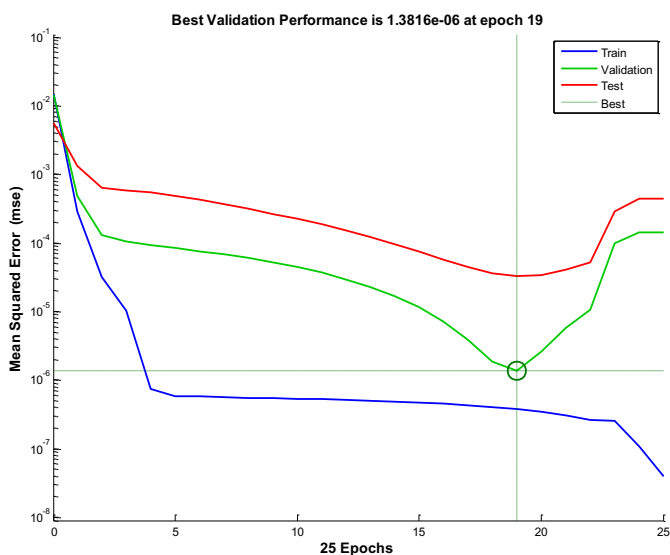
Figure 2: Performance of ANN training

For the purpose of electrical network modelling, data is obtained from the Croatian grid company HEP-ODS Elektroslavonija for a part of distribution network with a nominal voltage 35(20)kV and 0.4 kV with 48 terminals, 23 transformers and 25 different low-voltage loads. The distribution network is connected to the transmission network on two sides, but it is never doubly-fed due to operator technical conditions. If fully loaded, the voltage drops under 0.89 p.u.
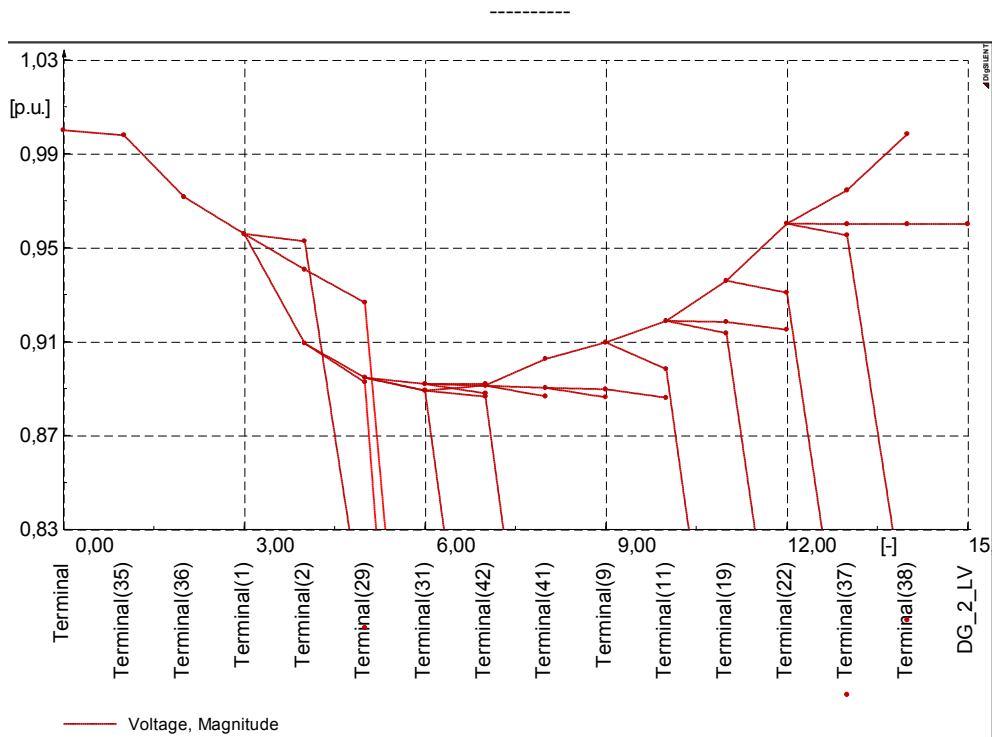
Figure 3: *Voltage values on terminals in fully loaded distribution network*

Of course, the normal operating conditions for this distribution network are not fully loaded terminals, and it is never doubly-fed, but it is necessary to observe what happens to voltage values. One possible solution for the increase of voltage values is planning for an adequate distributed generation on the convenient terminal in the system. In this case, the continuous electric power production would be as adequate a type as the stable source the network operator could rely on.

4   LOSSES ESTIMATION BY ANN

The ANN is modelled in MATLAB, which is a high-level language and interactive environment for numerical computation, visualization, and programming. After the ANN training, the fitting function and associated graph that shows how the results given by the ANN correspond to the control variables and results provided by DIgSILENT PowerFactory could be realized, as shown in Figure 4. The results provided by DIgSILENT PowerFactory power flow calculation are taken as correct real-life values since this software has previously and frequently proven its reliability and precision.
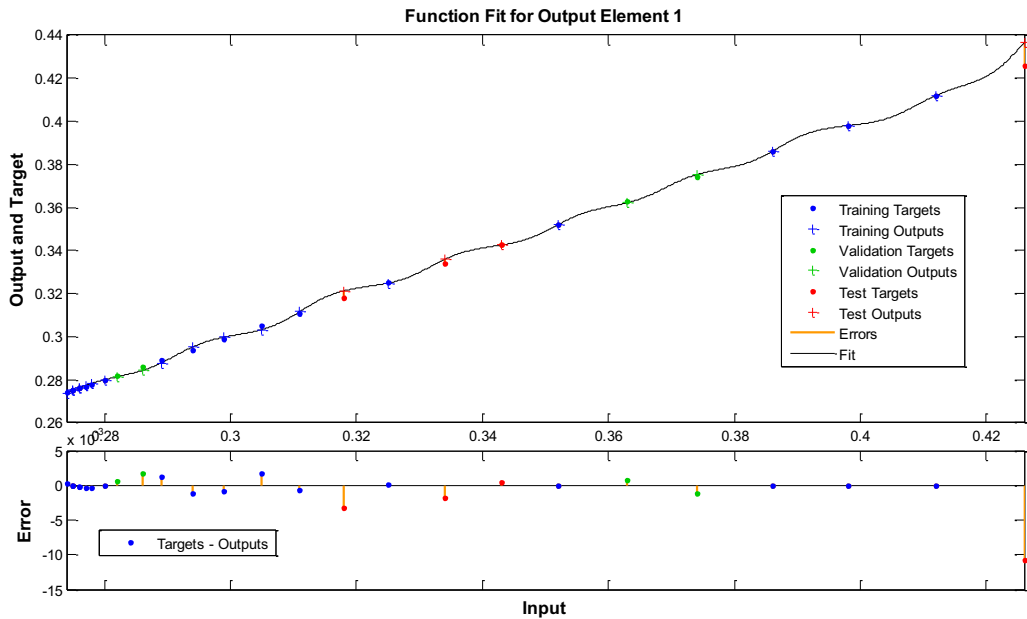
***Figure 4:** Fitting of the ANN*

The ANN is first tested on one terminal, randomly selected for DG implementation. The output of the ANN estimation is precise and accurate, regardless of on which number of implementation terminals and DG power it is tested.

By running the ANN on a set of variables for a selected terminal and running the power flow calculation in DIgSILENT PowerFactory software with same DG values, results can be compared and evaluated. The performance of the ANN is acceptable; the comparison of results given by DIgSILENT PowerFactory and by ANN after proper training shows that ANN manages to determine the valid value of power losses. The results of ANN are generally matching results provided by DIgSILENT PowerFactory. If the results should significantly deviate, the ANN has to be improved by managing the weight factors, biases and number of the hidden neurons. Furthermore, additional training data could be useful if improved precision would be a goal.

How the neural network response to input parameters can be shown by regression performance, as shown in Figure 5.

How the ANN estimates the influence on power losses and voltage control is shown in Table 1, where are shown compatible results of the calculation for one low voltage terminal, simultaneously made by ANN estimation and DIgSILENT calculation.
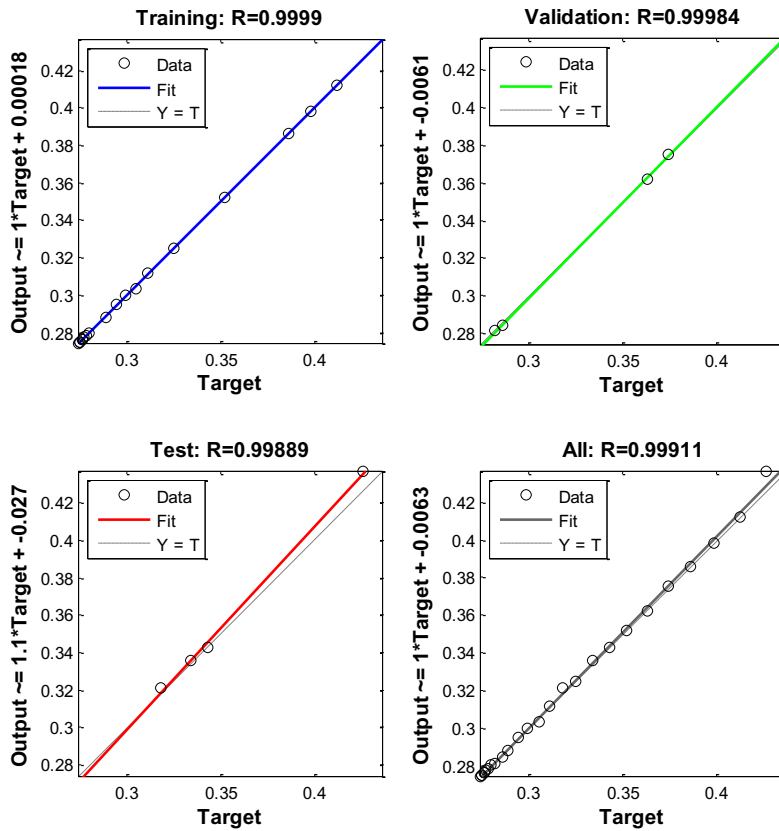
Figure 5: Regression of the ANN

The next step of determining the correct solution for minimizing active power losses and voltage level control is choosing the appropriate terminal and size of DG for implementation. This could be done analytically by comparing the results, by developing an additional ANN for decision making and choosing the correct terminal, or by developing a combined method that utilizes a genetic algorithm (GA) along with the ANN. In that case, the ANN is used for the assessment of the level of losses of the system, depending on the power of distributed generation and the terminal to which is it connected, and the GA is used to find the minimum solution.

Table 1: *Results of simulation in DIgSILENT and by ANN for one distributed generation terminal*

DG power production [kW]	Injected Current [kA]	Low Voltage Terminal [p.u.]	High Voltage Terminal [p.u.]	Active Power Losses [MW] **DIgSILENT**	Active Power Losses [MW] **ANN**
0,000	0.000	0.890	0.890	0.426	0.436788
100,000	1.481	1.000	0.975	0.412	0.411999

Optimization method for control of voltage level and active power losses based
on optimal distributed generation placement using Artificial Neural Networks
and Genetic Algorithms

150,000	1.424	1.000	0.976	0.398	0.398002
200,000	1.374	1.000	0.977	0.386	0.385997
250,000	1.329	1.000	0.978	0.374	0.375231
300,000	1.291	1.000	0.978	0.363	0.36217
350,000	1.261	1.000	0.979	0.352	0.352026
400,000	1.238	1.000	0.980	0.343	0.342537
450,000	1.222	1.000	0.981	0.334	0.335857
500,000	1.214	1.000	0.982	0.325	0.324879
550,000	1.215	1.000	0.983	0.318	0.321286
600,000	1.222	1.000	0.984	0.311	0.31163
650,000	1.238	1.000	0.985	0.305	0.303296
700,000	1.260	1.000	0.986	0.299	0.299777
750,000	1.288	1.000	0.986	0.294	0.295214
800,000	1.323	1.000	0.987	0.289	0.287773
850,000	1.363	1.000	0.988	0.286	0.284287
900,000	1.408	1.000	0.989	0.282	0.281378
950,000	1.457	1.000	0.989	0.28	0.280029
1000,000	1.444	1.000	0.990	0.277	0.277324
1050,000	1.566	1.000	0.991	0.276	0.276195
1100,000	1.625	1.000	0.992	0.275	0.27499
1150,000	1.687	1.000	0.992	0.274	0.273763
1200,000	1.750	1.000	0.993	0.275	0.27499
1250,000	1.816	1.000	0.994	0.275	0.27499
1300,000	1.833	1.000	0.994	0.276	0.276195
1350,000	1.952	1.000	0.995	0.278	0.278344

4.1   Optimal solution finding

Once all the data for every desired terminal in the system is generated, the optimal solution must be found; doing so is a decision-making process that has to be properly designed. In recent years, increasing research efforts have been directed at applying ANN to decision-making tasks and mixed opinions about the value and performance of this technique have emerged: from considering ANN effective for unstructured decision making to categorically expressing reservations towards decisions made by artificial intelligence. The ANN for decision making and optimal solution finding is not used in this paper.

The genetic algorithm is becoming increasingly represented in optimization with non-linear dependences; it is an adaptive heuristic search algorithm introduced on the evolutionary themes of natural selection, [3]. In this case, the starting population could be that of potential (or all) terminals on which the selection would be performed. In such cases, the main condition that would need to be met is the well-defined fitness function of each terminal. [9]

Along with the GA, there are other types of soft-computing methods that could be used to find the best solution. Methods proven to be exceptionally good include Swarm Intelligence or Particle Swarm Optimization and Ant Colony Optimization, since they are efficient in the optimization of problems in a search space, [2]. Finally, the well-known Fuzzy Controller could be implemented, which could, if designed correctly, prove to be the most robust yet still simple design.

5   GENETIC ALGORITHM AND ANN HYBRID METHOD

Representation of results has to be a fixed-length bit string in order for GA to function. Each position in a string is assumed to represent a particular feature of an individual solution. The value stored in that particular position shows how one feature is evaluated in solution. In the specific requirements for the purpose of this paper, operation scenarios are divided by the power of implemented DG and by the number of connected terminals. The arrangement of operation scenarios in the number of the population can be determined in several ways. The authors of this paper used DG power as a difference from each population. Individuals in each population differ from each other by connected terminal.

The arrangement of the population and individual coding is shown on Figure 6.

Individual on i-th terminal
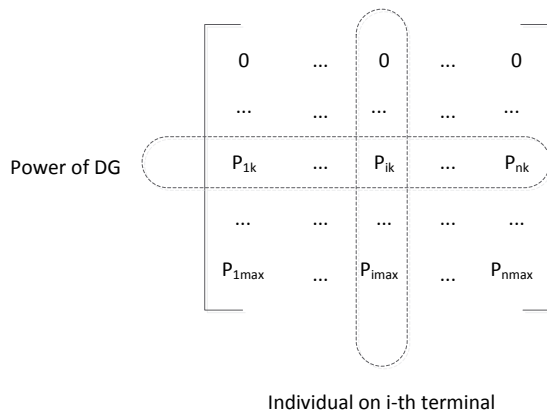
Figure 6: *Arrangement of population and individual coding*

For the purpose of future research, the task of developing a method that could utilize each terminal as a population, where individuals of that population are represented with different DG power, remains to be completed. The proposed method is represented by the algorithm shown on Figure 7; it uses GA and ANN to find the best solution.
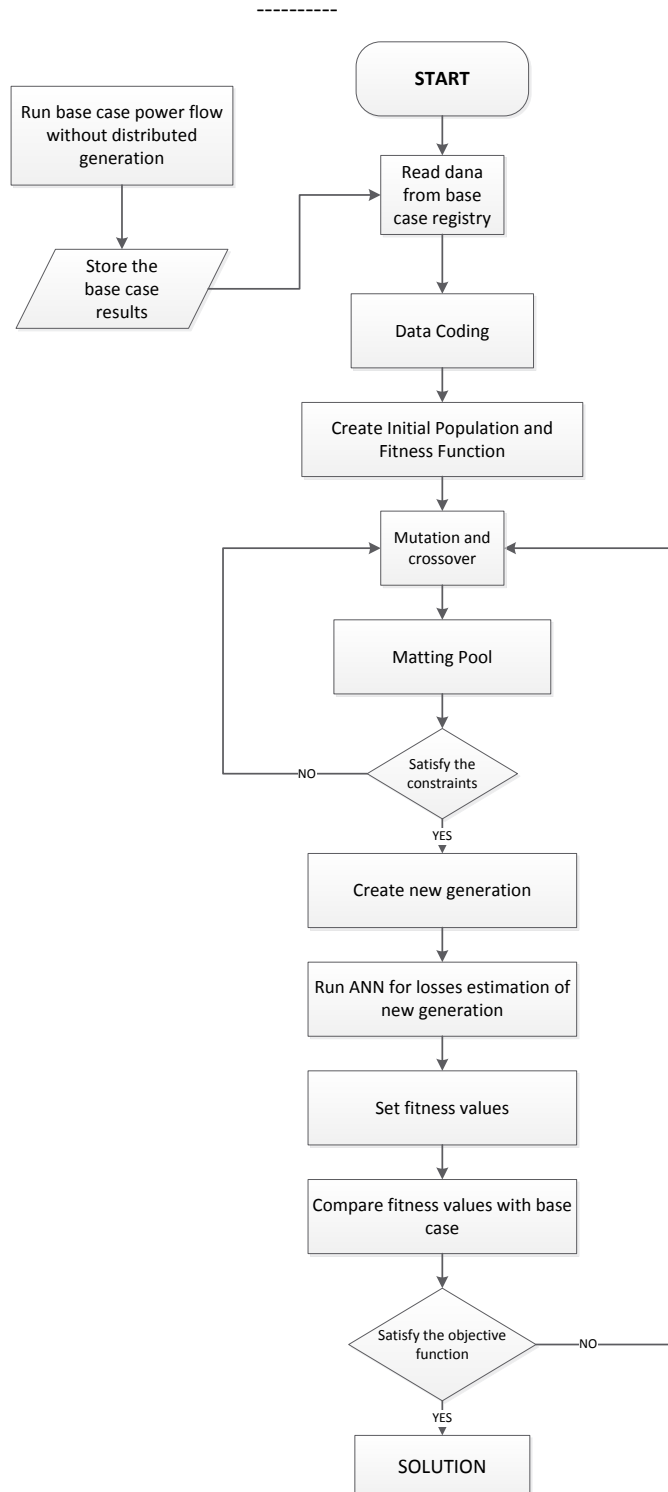
Figure 7: *Algorithm of proposed method*

----

6   THE METHOD APPLICATION IN DISTRIBUTION SYSTEM

6.1 System description

Figure 8 shows a 48-terminal system used for the purpose of modelling and testing of proposed methods. The network has the possibility of being doubly-fed, but the real operation conditions are usually two single-fed feeders. For the purpose of this paper, the worst case operation scenario is provided: a doubly-fed, fully-loaded distribution network. The constraints given in the previous chapter are fully satisfied in power flow calculation by DIgSILENT PowerFactory for every level of DG power.
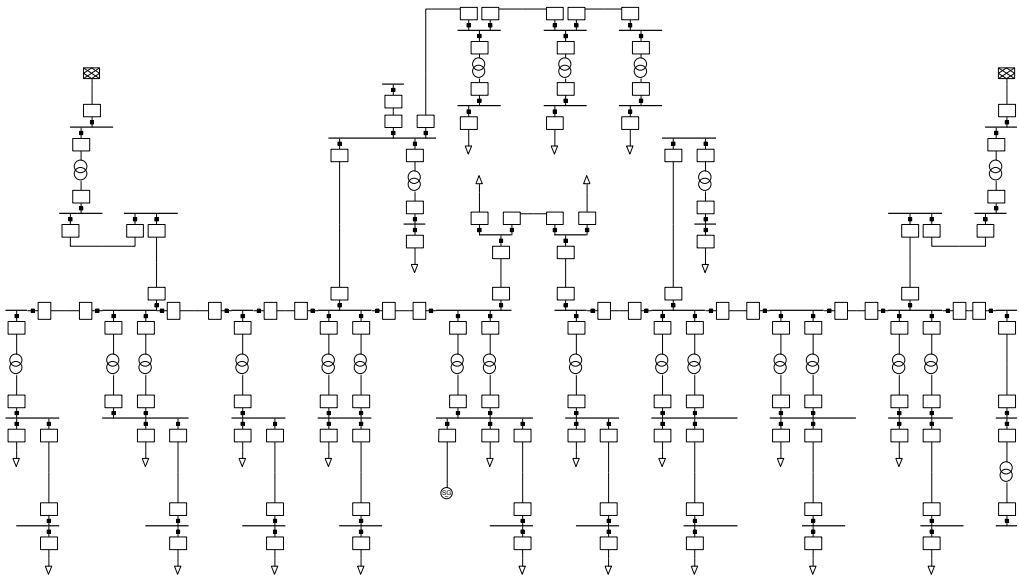
Figure 8: Single line diagram of the 48-terminal distribution system considered

6.2 Load model

The total installed peak power demand in the system is 2.59MVA with an average power factor of 0.9. The conditions considered by the research of this paper are peak loaded network with load diversity factor of one. The simulation and performance evaluation of the proposed method has been conducted for time-independent loads and time-independent generation.

6.3 Distributed generation

There are different types of DG, differed by their energy source and time-dependent production, [10]. In this paper, DG is modelled as a PQ node, with a power factor of cos φ = 1, and power that can vary from 100kW to 1350kW. The selected type of DG is based on a real type of generator widely used in distributed production worldwide. For the purpose of this

Optimization method for control of voltage level and active power losses based
on optimal distributed generation placement using Artificial Neural Networks
and Genetic Algorithms

----

model, the Stamford generator with nominal power of 1350kW, 1500 min^{-1} is chosen, as a part of a GE Gas Engine solution.

6.4 Performance evaluation and results

Resulting simulations and all implemented calculations designed in the proposed algorithm can be represented with surface diagram shown in Figure 9.
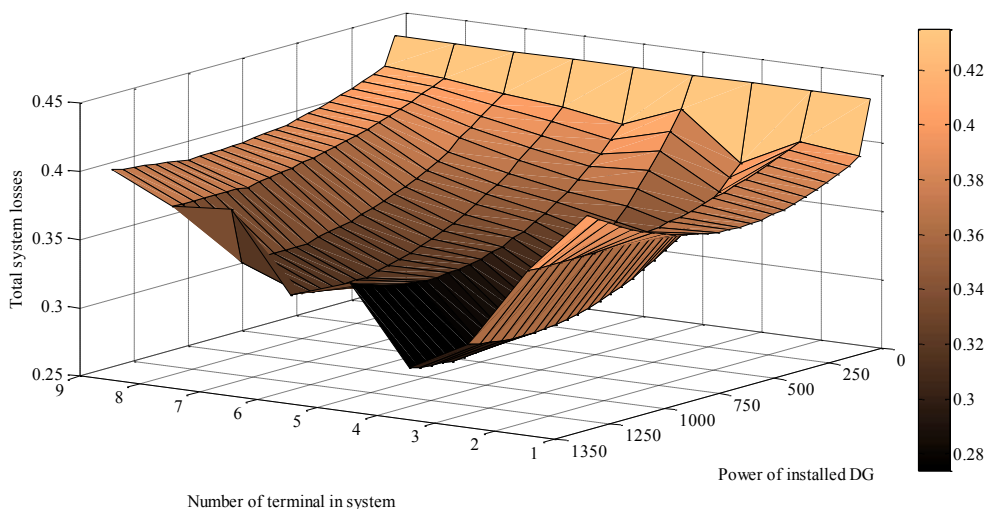
Figure 9: *Surface diagram of scenarios analysed by GA*

The surface diagram of results obtained via GA clearly indicates the global minimum of the values set. The dark area represents the set of optimal solutions according to the optimization formulation defined earlier in this paper. The power of DG from 1100kW to 1250kW causes the lowest level of total active power losses in the analysed system and the best result of DG placement and power selection. This indicates the result with the lowest system losses, 1150kW DG on Terminal 8 located in the middle of the distribution feeder, on the fifth set of low voltage terminals from 10 sets. A GE Gas Engine with Stamford generator is entirely capable of providing such a power level. Total active power losses before installing DG in the distribution system were 468kW; after implementing the DG on designated terminal, total system losses were 274kW, or 41.4% lower.

The proposed solution provided by the GA and ANN method is evaluated with DIgSILENT PowerFactory software in order to check the accuracy of results. In accordance with these requirements, the generator is modelled in DIgSILENT PowerFactory on Terminal 8, with 1150kW installed power. Power flow calculation is performed for that operation scenario, and a significant improvement in active power losses reduction and regulation of voltage values on each terminal are observed and confirmed.

The voltage values in the modelled network have been improved significantly; the lowest voltage level for this operation scenario was 0.95 p.u, (Figure 10), but before DG

----

implementation the lowest voltage level was 0.88 p.u. Regardless of the DG implementation terminal, the voltage level never exceeded upper technical limit of 1.1 p.u.
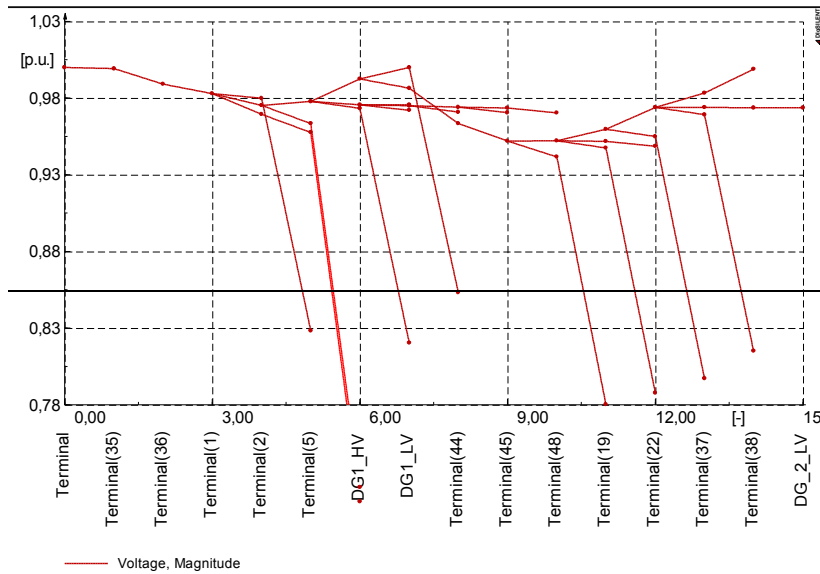
Figure 10: *Voltage values on terminals with 1150kW DG on Terminal 8*

DIgSILENT PowerFactory calculated the total active power losses of 273kW, which is remarkably close to the results for the same scenario estimated by ANN. Since the improvement of voltage value and the active power losses control is achieved, the proposed method of combining GA and ANN could provide a real-time solution for the economical operation of distribution systems.

7   CONCLUSIONS

Distributed Generation (DG) is increasingly common in electrical distribution networks, so its influence needs to be properly evaluated and rated in order to achieve the greatest benefit for DG itself as well as for the power system. A new optimization method based on Artificial Neural Networks (ANN) and Genetic Algorithms (GA) is proposed in this paper, and how the method could be used for the determination of size and location of DG is successfully demonstrated. This method is based on formulation by objective function and technical constraints. The rapidly obtained and correct solution for solving the given formulation is provided by using ANN, since they have the ability to solve non-linear mathematical problems extremely quickly and precisely. Back-propagation ANN is designed and trained via power-flow calculation results provided via DIgSILENT PowerFactory software for estimating the active power losses in the distribution system. In addition, GA is used for finding the best optimal solution, i.e. the one with the lowest active power losses, based on the best fitness performance of each individual in each population. Populations differ from each other by the power of DG, and individuals differ from each other by the terminal to which they are connected.

*Optimization method for control of voltage level and active power losses based
on optimal distributed generation placement using Artificial Neural Networks
and Genetic Algorithms*

Improvements in voltage profiles and active power losses reduction made by the proposed method confirm the usefulness of the combination of ANN and GA for radial and networked distribution systems.

References

[1] **S. Biswas, S.K. Goswami, A. Chatterjee**: *Optimum distributed generation placement with voltage sag effect minimization*, Energy Conversion and Management, Elsevier, 2012.

[2] **K.S. Swarup, P.S. Subash**: *Neural network approach to voltage and reactive power control in power systems*, Intelligent Sensing and Information Processing, International conference, 2005,

[3] **S. Sumathi, P. Surekha**: *Computational Intelligence Paradigm – Theory and applications using Matlab®*, CRC Press, Taylor & Francis Group, 2010.

[4] **A.A. Abour El-Ela, Sm. M. Allam, M.M. Shatla**: *Maximal optimal benefits of distributed generation using genetic algorithms*, Electric Power System Research, vol.80, 2010., pp.869–877

[5] **E. Rezenia, S.M. Shahidehpur**: *Real Power loss minimization using interior point method*, Electric Power and Energy Systems, vol.23, 2001, pp. 45–46

[6] **K. Byeong-Gi , R. Dae-Seok**: *Optimal Voltage Regulation Method for Distribution Systems with Distributed Generation Systems Using the Artificial Neural Networks*, JEET, vol. 8, No 742, 2013.

[7] **H. Gavin**: *The Levenberg-Marquardt method for nonlinear least squares curve fitting problem*, Duke University, 2011.

[8] *DIgSILENT PowerFactory User's Manual*, Vol. I & 2, Edition 1, DIgSILENT GmbH, 2011.

[9] **D. Lukman, T.R. Blackburn**: *Modified Algorithm Of Load Flow Simulation For Loss Minimization In Power Systems*, IEEE/PES, Sydney, 2003.

[10] **Y. Alinejad-Beromi, M. Sedighizadeh, M.R. Bayat, M.E. Khodayar**: *Using genetic algorithm for distributed generation allocation to reduce losses and improve voltage profile*, International Universities Power Engineering Conference - UPEC. 2007. pp. 954–959

[11] **J.M. Abdallah, A.R. Al-Zyoud**: *Voltage and Reactive Power Control Simulations Using Neural Networks*, IJSSST, vol.10, No.4, pp. 64–72

[12] **M. Vardarajan, K.S. Swarup**: *Differential evolutionary algorithm for optimal reactive power dispatch*, Electric Power and Energy Systems, vol. 30, 2008, pp. 435–441

[13] **S.M. Moghaddas-Tafreshi, H.A. Zamani, S.M. Hakimi**: *Optimal sizing of distributed resources in micro grid with loss of power supply probability technology by using breeding particle swarm optimization*, J. Renewable Sustainable Energy 3, 2011

[14] **A.Q.H. Badar, B.S. Umre, A.S. Junghare**: *Reactive power control using dynamic Particle Swarm Optimization for real power loss*, Electric Power and Energy Systems, vol.41, 2012., pp. 133–136.

----

[15] **S. M. Hakimi, S. M. Moghaddas-Tafreshi, H. HassanzadehFard**: *Optimal sizing of reliable hybrid renewable energy system considered various load type*, J. Renewable Sustainable Energy 3, 2011

[16] **S.M. Moghaddas-Tafreshi, Elahe Mashhour**: *Distributed generation modeling for power flow studies and a three-phase unbalanced power flow solution for radial distribution systems considering distributed generation*, Electric Power Systems Research, Volume 79, Issue 4, p.680–686, 2009.

[17] **W-S. Tan, M.Y. Hassan, M.S. Majid, H.A. Rahman**: *Optimal distributed renewable generation planning: a review of different approaches*, Renewable and Sustainable Energy Reviews 18, pp. 626–645.

[18] **R.K. Singh, S.K. Goswami**: *Optimum allocation of distributed generations based on nodal pricing for profit, loss reduction, and voltage improvement including voltage rise issue,* Electric Power and Energy Systems, vol. 32, 2010., pp.637–644

[19] **N-C. Yang, T-H. Chen**: *Evaluation of maximum allowable capacity of distributed generations connected to a distribution grid by dual genetic algorithm*, Energy and Buildings, vol. 43, 2011., pp. 3044–3052.

[20] **M.R. AlRashidi, M.F.AlHajri**: *Optimal planning of multiple distributed generation sources in distribution networks: A new approach*, Energy Conversion and Management, vol.52, 2011., pp. 3301–3308.

NUMERICAL ANALYSIS OF FLOW OVER A WIND TURBINE AIRFOIL

NUMERIČNA ANALIZA TOKA OKOLI LOPATIČNEGA PROFILA VETRNE TURBINE

Janez Bitenc[ℜ], Brane Širok, Ignacijo Biluš

Abstract

This work presents a comparison of flow conditions over a NACA 4421 two-dimensional airfoil with a closed trailing edge (normal airfoil shape) and a new blade shape with an open trailing edge. The numerical analysis was made using software for an approximate solution of a system of conservation law equations. The results yield a comparison of numerically obtained values of the lift coefficient, as well as diagrams of pressure coefficients and velocity vectors on the airfoil, at different angles of attack. The validity of the method of computation was confirmed with a comparison of computed lift coefficient values for the closed trailing edge profile, with experimentally acquired values from literature. It is reasonable to continue the research of flow conditions with the use of the open trailing edge airfoil.

Povzetek

Predstavljena je primerjava tokovnih razmer pri obtekanju zraka okoli dvodimenzionalnega profila NACA 4421 z zaprtim izstopnim robom (običajna oblika profila) in novo obliko lopatice z odprtim izstopnim robom. Numerična simulacija je bila narejena s programskim paketom za aproksimativno reševanje sistema parcialnih enačb, ki predstavljajo ohranitvene zakone. Rezultati podajajo primerjavo izračunanih vrednosti vzgonskih koeficientov, ter diagrame tlačnih koeficientov in vektorjev hitrosti na profilu, za različne natočne kote. Pravilnost načina izračuna je bila potrjena s primerjavo izračunanih vrednosti koeficientov vzgona za primer zaprtega

---

[ℜ] Corresponding author: Janez Bitenc, Tel.: +386 41 800 668, Mailing address: Ul. Janka Kača 2, SI-3310 Žalec, Slovenia
E-mail address: jbitenc@icloud.com

----

profila, z eksperimentalno pridobljenimi vrednostmi iz literature. Rezultati simulacij kažejo, da je smiselno nadaljevanje raziskav izboljšanja tokovnih razmer z uporabo lopatice z odprtim izstopnim robom.

1   INTRODUCTION

Wind turbines are propulsion engines for exploiting renewable energy sources. Wind turbine rotors are divided into drag-based and lift-based or horizontal and vertical, [1]. They are unable to convert the total energy from wind into mechanical work. The theoretical aerodynamic efficiency factor is called the Betz limit and is 59.3%. The motivation for these computations were the current efficiency factors with which conventional wind turbines are operating, which are much lower than the Betz limit and highly dependent on the flow conditions around airfoils.

This article discusses the airflow over wind turbine airfoils, for conventional and new blade shapes. Because different angles of attack and blade shapes lead to different flow conditions and thus significantly affect lift and drag coefficients, the discussion is limited to C_L and C_p computation for the profile in external flow. The goal was to show that the new blade type ensures more favourable flow conditions. As a new blade type, a hollow blade, [2], is introduced, with air flow streaming from the trailing edge of the profile, with which we wish to increase the lift coefficient and prevent the intrusion of secondary flow along the blade suction side in the trailing edge area. Numerical simulations of flow conditions were made with Ansys CFX software.

2   WING THEORY

The maximum obtainable power of the wind turbine in a free stream, which is independent of the design of wind turbine, is known as Betz's law. It is derived from the conservation laws of the mass and momentum of the airflow that passes through the idealized actuator disk, which extracts energy from the air stream. According to Betz's law, it is impossible for a wind turbine to take advantage of more than 59.3% of kinetic energy of the wind. In practice, wind turbines reach their peak at 75–80% of the Betz limit.

2.1   Betz limit

The Betz limit represents the ratio between the maximum achievable power of the turbine and the wind power. It equals, [3]:

$$\eta_{maks} = \frac{P_{maks}}{P_{tot}} = \frac{8}{27} \cdot 2 = 0.5926 \tag{2.1}$$

Where

$$P_{maks} = \frac{8}{27} \rho A v_\infty^3 \tag{2.2}$$

$$P_{tot} = \frac{1}{2} \rho A v_\infty^3 \tag{2.3}$$

----

and

$v_\infty -$ *wind speed,*
$A -$ *rotor disc area,*
$\rho -$ *air density.*

Therefore, this is the maximum efficiency of wind turbines: no more than 60% of the kinetic wind energy can be converted into mechanical work, [3].

Figure 1 shows the efficiency factors of some of the practical implementations of wind turbines. On the abscissa are lined up tip speed ratios λ, representing the ratio between tip speed u and free stream airflow v_∞, [3]:

$$\lambda = \frac{u}{v_\infty} = \frac{2\pi nR}{v_\infty} \tag{2.4}$$

From the graph in Figure 1, we can see that the efficiency of wind turbine greatly depends on the tip speed ratio and rotor type. For values $\lambda < 2$, the efficiency is even in optimal conditions greatly lower than the values of $\lambda > 5$ where we obtain the maximum efficiency factors. This difference is even more obvious in actual wind turbines. The greatest efficiency factors are possible to achieve in the narrow optimal tip speed ratio interval, where the numbers range between $\eta = 0.30$ and $\eta = 0.40$, [1].
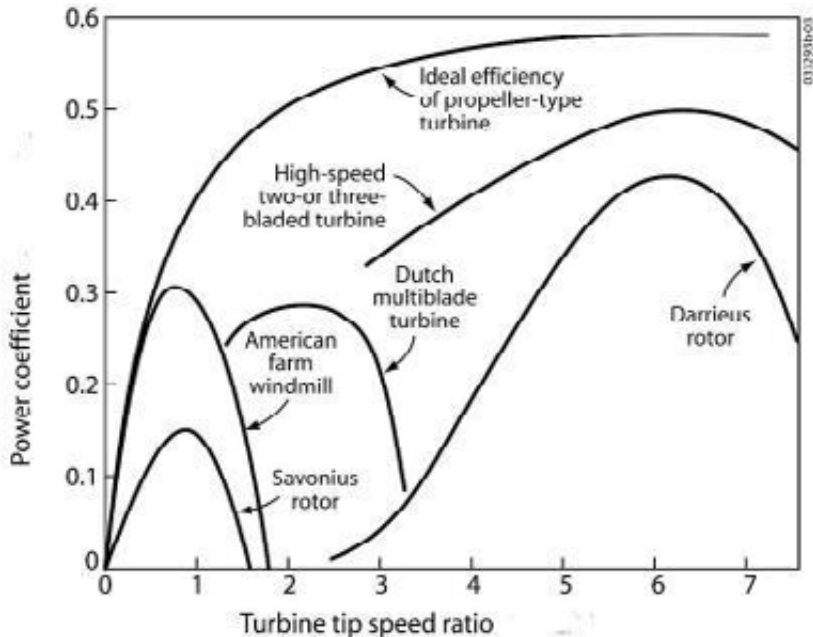
Figure 1: Comparison of efficiency factors of some of the practical implementations of wind turbines in relation to tip speed ratio, [1]

2.2   Aerodynamic forces and moments

Regardless of complexity of the studied model, the sources of aerodynamic forces and torque on the wing profile in the outer flow, pressure and shear stress distributions are at the airfoil. As shown in Figure 2, the pressure acts perpendicularly, and the shear stress tangentially on the surface. Shear stress is the result of friction between air and body surface, [3].
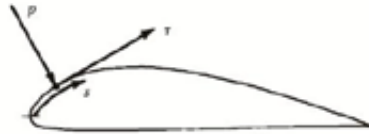
Figure 2: Distribution of pressure p and shear stress τ along the profile, [3]

The final effect of the distribution of p and τ, integrated over the whole body surface, is the resultant of aerodynamic forces R and momentum M on the body, as shown in Figure 3.
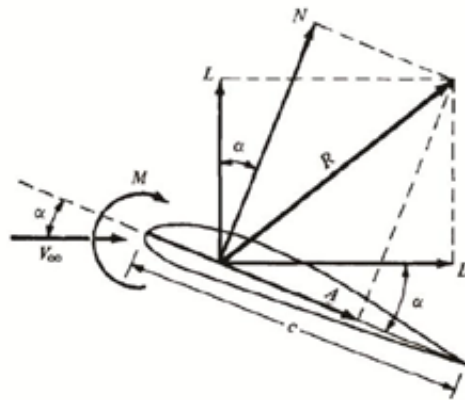
Figure 3: Resultant of aerodynamic forces on the profile, its components and momentum

The resultant forces R can be divided into components; two pairs are represented in Figure 3. Speed v_∞ is the free stream speed.

In Figure 3, by definition, the marked forces are, [3]

L is lift force. It is the component of resultant force R, perpendicular to v_∞

D is drag force. It is the component of resultant force R, parallel to v_∞

N is normal force. It is the component of resultant force R, perpendicular to c

A is axial force. It is the component of resultant force R, parallel to c

The relation between L and N, as well as D and A gives the equations [3]

$$L = N \cos \alpha - A \sin \alpha \qquad (2.5)$$

$$D = N \sin \alpha - A \cos \alpha \qquad (2.6)$$

2.3 Dimensionless coefficients

Lift force is the result of change in the momentum of the air as it streams onto the blade. Drag force is the result of friction and pressure differences. Usually, they are represented with lift C_L and drag coefficients C_D,[1]

$$C_L = \frac{L}{\frac{1}{2} v_\infty^2 \rho_\infty S} \qquad (2.7)$$

$$C_D = \frac{D}{\frac{1}{2} v_\infty^2 \rho_\infty S} \qquad (2.8)$$

where L and D are lift and drag forces (Equations 2.5 and 2.6), v_∞ flow velocity and S wing area. Both coefficients are dependent on flow conditions, which are primarily determined by the angle of incidence α, [1].

Another influential dimensionless coefficient is the pressure coefficient C_p

$$C_p = \frac{p_\infty}{\frac{1}{2} v_\infty^2 \rho_\infty} \qquad (2.9)$$

2.4 Flow separation and the impact on the lift coefficient

With increasing air velocity or increasing values of the Reynolds number, the boundary layer along the profile changes. Speed distribution in the boundary layer is dependent on shear forces τ, acting along the wall (Figure 4).
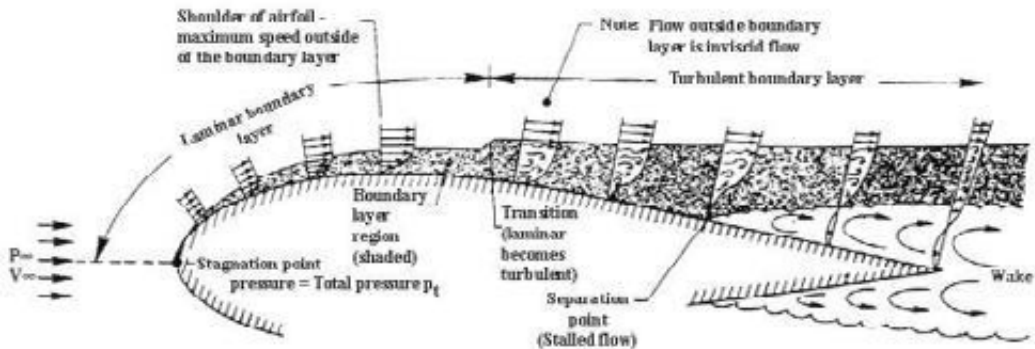
Figure 4: Development of boundary layer along the wing profile, [4]

The boundary layer is initially laminar, but depending on the Reynolds number and angle of attack α, it becomes unstable at a certain distance from the leading edge, where it develops into turbulent boundary layer. The effect of pressure gradient on the boundary layer is evident from Figure 4. Downstream, it has enormous impact on flow conditions along the wall and thus on the flow separation. Velocity increases behind the leading edge, where the profile widens. In contrast, the velocity lowers in the area of profile narrowing. Consequently, on the front of the profile the pressure lowers and increases towards the trailing edge, [5].
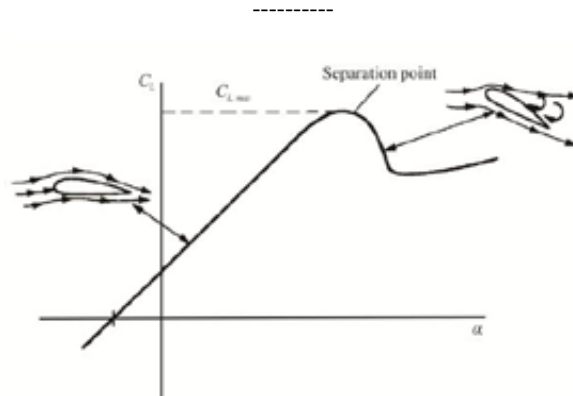
Figure 5: *Example of lift coefficient change in relation to angle of attack, [3]*

The lift coefficient increases linearly until a critical angle is reached and the maximum lift coefficient is achieved. The point at which tearing of the boundary layer and flow swirling occurs is called the flow separation point. At that moment, the lift coefficient suddenly drops and the lift force collapses (Figure 5), [3].

The purpose of this study was to analyse the impact of the new blade shape on the flow separation point and consequently on the airfoil lift coefficient.

3   NUMERICAL SIMULATION

3.1   The governing equations

The numerical simulation was made using RANS (Reynolds Averaged Navier-Stokes) method combined with the two equation turbulence model. The governing equations are:

- continuity equation

$$\boldsymbol{\nabla} \cdot \boldsymbol{U} = \frac{1}{\rho}\dot{m} \tag{3.1}$$

- momentum equation

$$\frac{\partial(\rho\boldsymbol{U})}{\partial t} + \boldsymbol{\nabla} \cdot (\rho\boldsymbol{U}\boldsymbol{U}) = -\boldsymbol{\nabla}P + \boldsymbol{\nabla} \cdot \tau + S_M \tag{3.2}$$

In the equation system above, $\boldsymbol{U}$ [m/s] represents the time averaged mixture velocity, P [Pa] is the time averaged pressure, ρ [kg/m^3] is density, τ [N/m^2] is stress tensor and S_M [kg/m^{2}s^2] are momentum sources.

In order to close the set of governing equations, additional modelling is required to compute the turbulence quantities. The turbulence quantities were modelled using a conventional *SST* model.

3.2   Geometry and meshing

NACA 4421 profile, [6], was used for the computation for different angles of attack α. Meshing was conducted with ANSYS ICEM software. The domain is rectangular in shape and shown in Figure 6. The main dimensions, rounded to the nearest whole number, are:

- Domain length is 6.7201·c [m],
- domain height is 3.3036·c [m],
- distance from the profile leading edge to front wall of the domain is 1.6518·c [m].
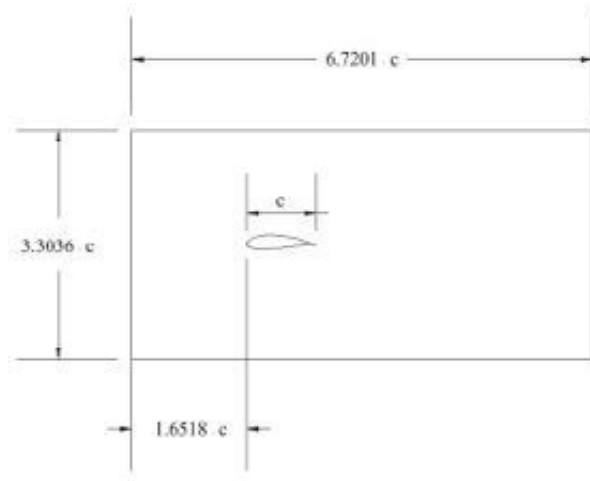
Figure 6: *Domain and profile dimensions in meters [m]*

Two numerical analyses of flow over closed and open trailing edge profiles were made. In the first, data from the literature have been used, [6]. The chord lengths c are:

- chord length of closed trailing edge profile is c = 3.027 m,
- chord length of open trailing edge profile is c = 2.927 m.

In second, the angle of attack was fixed at α = 3° and the analysis was made for three different domain inlet and profile outlet velocities, [7].

Chord lengths c are:

- chord length of closed trailing edge profile is c = 0.03027 m,
- chord length of open trailing edge profile is c = 0.02927 m.

To determine the appropriate mesh, a nodal analysis was made. Three mesh densities were made, for four angles of attack. The obtained results were compared with experimental ones [6]. The middle mesh density was chosen; the details of it are:

- number of nodes: 176,000,
- number of elements: 87,000.

3.3   Numerical simulation parameters

For the computation of wind turbine airfoil characteristics, a steady-state simulation was used. A graph of experimentally obtained lift coefficient values for the Reynolds number of $3 \cdot 10^{6}$ was used as a reference data, [6].
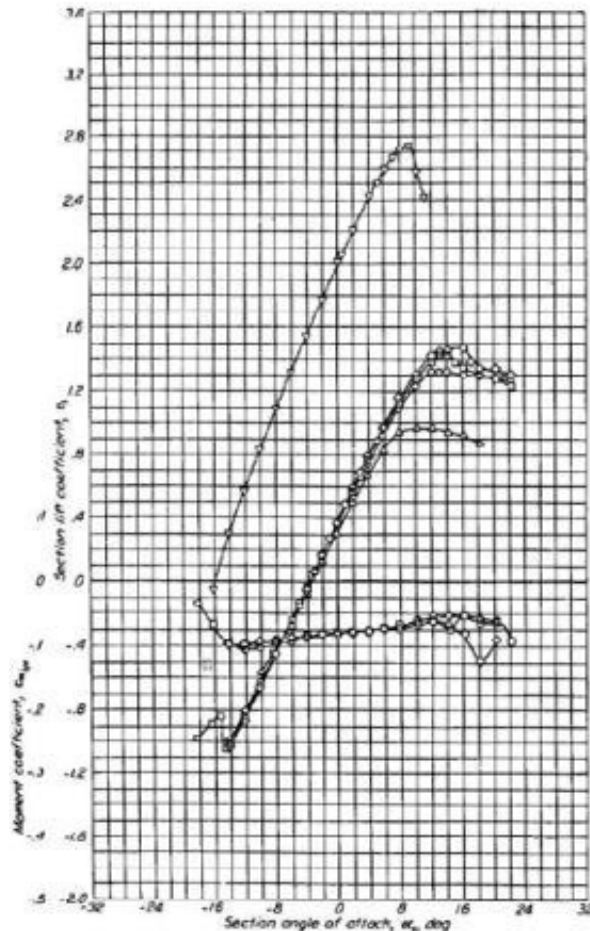
Figure 7: NACA 4421 lift coefficients; ''○'' indicates results at Re = 3.0· 106, [6]

The outlet velocity on the trailing edge of an opened profile was 12 m/s. The fluid used was air at a temperature of 25° C and ambient pressure of 101325 Pa. Due to potential reversed vortices, the outlet edge of the domain was defined as "opening", at a pressure of 0 Pa. The upper and lower sides of the domain, as well as suction and pressure sides of the profile, were defined as a "no-slip wall". Boundary conditions are shown in Figure 8. The SST turbulent model was used, which provides more accurate results about events along the wall, due to its properties.
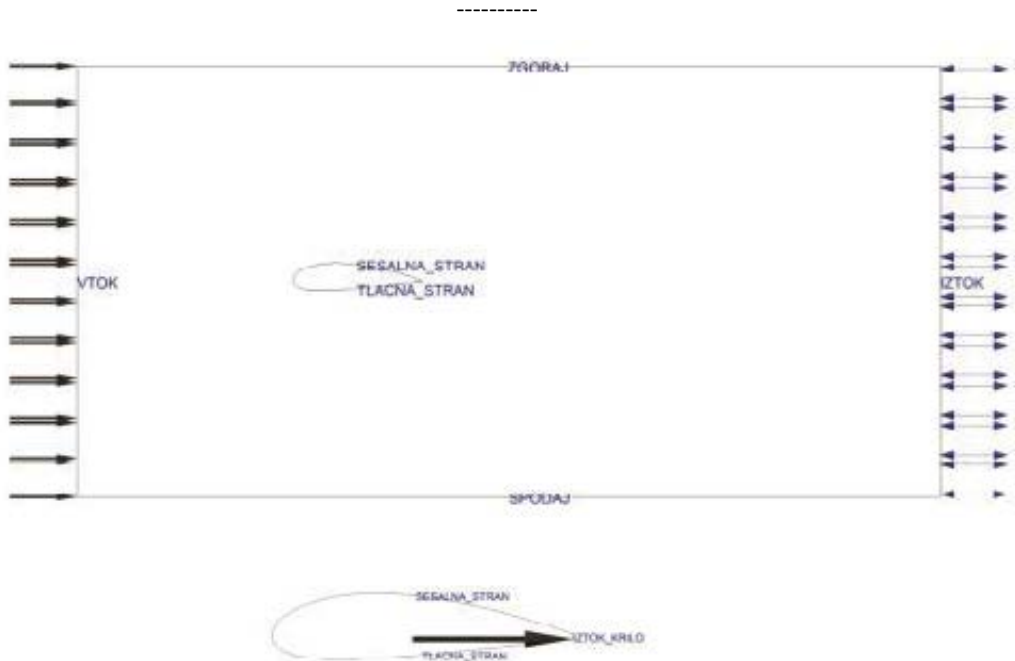
Figure 8: *Boundary conditions for closed trailing edge (above) and open trailing edge profile (below). Domain boundary conditions are in both cases the same*

At a α = 3° angle of attack, a numerical analysis of flow for the closed and open trailing edge profile was made at three different inlet and outlet velocities. Inlet velocity was defined in the form of a developed flow profile. The open trailing edge outlet velocity v_i, was determined as a value of speed function at the point y = -0.035 (maximal velocity) and reduced by a certain percentage.

4   RESULTS AND DISCUSSION

4.1   Comparison of lift coefficients

The computed data was compared with experimentally obtained values of C_L, [6], shown in Figure 7.

Figure 9 presents the comparison of computed values of C_L for both types of profiles, with the experimentally obtained values.
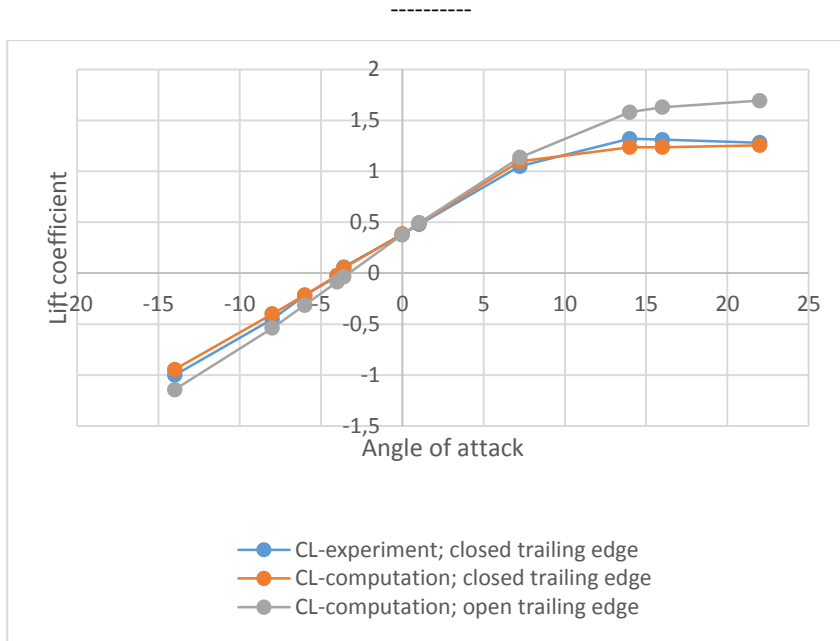
Figure 9: *Comparison of lift coefficients*

Good correlation of experimental and computed values for basic profile (closed trailing edge profile) is evident from the diagram above, as well as increase of lift coefficient in the case of an open trailing edge profile.

4.2   Comparison of pressure coefficients

In Figures 10 to 13, comparisons of pressure coefficient C_p and shear stress for both types of profiles are given, at angles of attack α = 7.24° and α = 14°.
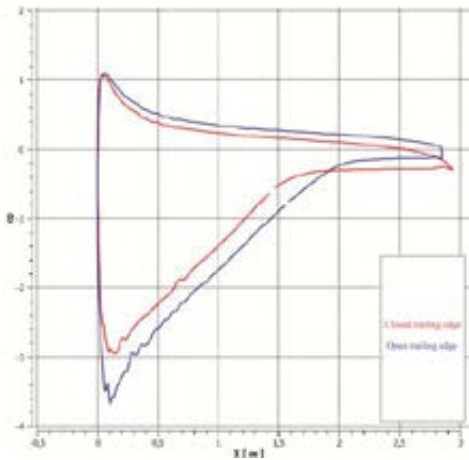
Figure 10: *Pressure coefficient; α = 14°*
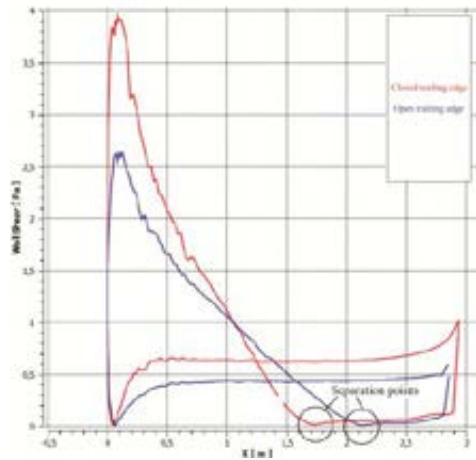
Figure 11: *Shear stress; α = 14°*
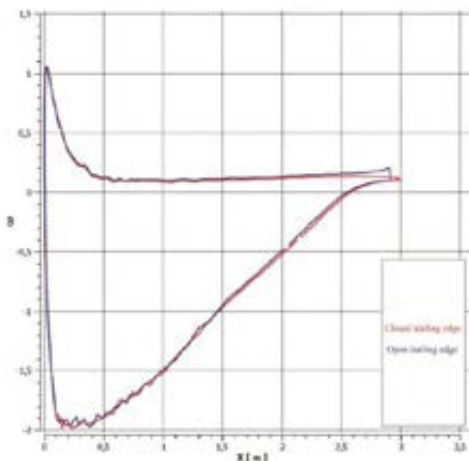
Figure 12: *Pressure coefficient; α = 7.24°*
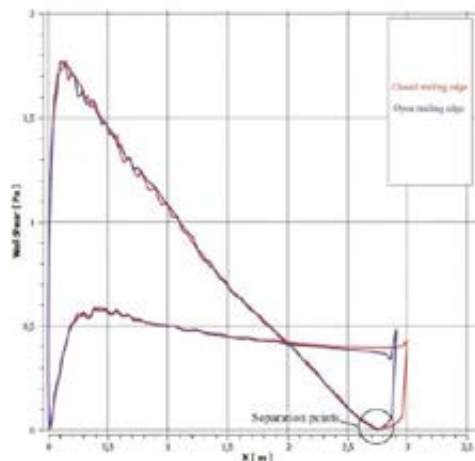
Figure 13: *Shear stress; α = 7.24°*

From Figures 10 and 12, it is evident that the negative values of pressure coefficient present greater lift force, because the lowering of the pressure on the suction side means a greater pressure difference. Separation points are evident from Figures 11 and 13, in which the shear force equals zero. At absolute values of separation points, the shortening of the blade because of a cut trailing edge needs to be taken into account.

Figure 14 shows velocity vectors at angles of attack 14° and 7.24°. A later beginning of flow swirling at the open trailing edge profile is evident, which indicates a movement of the separation point towards the trailing edge of the profile.

(a)   (b)
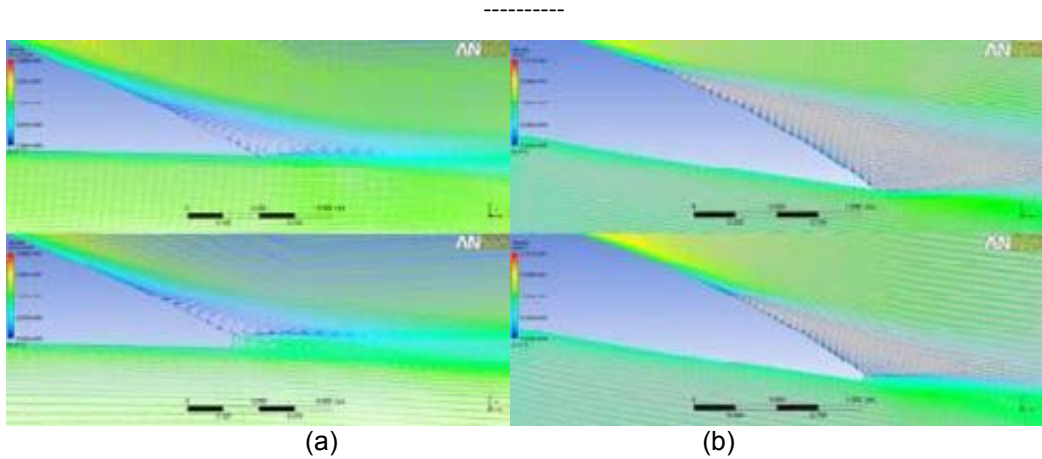
Figure 14: *Comparison of velocity vectors along the profile at angles of attack α = 14° (a)*
and α = 7.24° (b)

4.3 Impact of air velocity change on the results

In Table 1 and in Figure 15 andFigure 16, the results of numerical analysis for closed and open trailing edge profiles, at an angle of attack of 3° and three different inlet and outlet air velocities are shown.

Table 1: *C_L at angle of attack α = 3°*

	Velocity v_1	Velocity v_2	Velocity v_3
C_L for closed trailing edge profile	0.0486	0.0495	0.0504
C_L for open trailing edge profile	0.0856	0.0916	0.0963
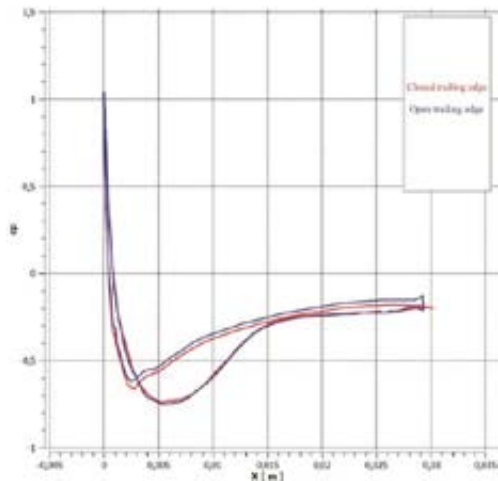
Figure 15: *Pressure coefficient at air velocity v_1 and angle of attack α = 3°*   **Figure 16:** *Pressure coefficient at air velocity v_3 and angle of attack α = 3°*
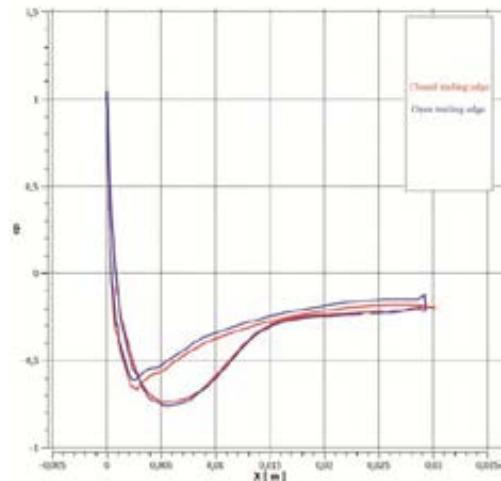
From the results, it is evident that lift coefficients are raised in accordance to velocity. The difference between C_L for closed and open trailing edge profile is not the same, but rises with the rising of the velocity. Figure 15 and Figure 16 show the comparison of pressure coefficients of close and open trailing edge profiles. Because of the small values of C_L, differences between C_p are barely noticeable.

5   DISCUSSION

The end results of the numerical analysis of flow over wind turbine airfoil indicate an improvement of flow conditions in case of open trailing edge airfoil, for angles of attack of $α > 0°$. At angles $α ≤ 0°$, the lift coefficients deteriorate, because of the flipped flow conditions on the suction and pressure sides.

The values of lift coefficient for closed and open trailing edge profiles give the typical lift coefficient distribution, which raises linearly with an increasing angle of attack and begins to drop when a critical angle of attack is attained. From the presented figures, it is clear that the computationally obtained values correlate well with experimental data. Later flow separation is evident in the case of the open trailing edge profile, especially at greater angles of attack. The average percentage of lift coefficient increase in case of the new blade type is (for the discussed angles of attack greater than 0°): approximately 15%. The results of the numerical analysis at an angle of attack of 3° and three different velocities showed that with proportional increases of air velocity at the domain inlet and the open trailing edge outlet, lift coefficient also increases. C_L in case of open trailing edge profile is on average 52% greater than in case of closed trailing edge profile.

Given the above, we can conclude that the open trailing edge profile favourably impacts flow conditions.

----

6   CONCLUSIONS

At default simplifications (2D model, stationery flow field, ignoring the kinetic energy of flow through the open trailing edge on the C_L formula), it was found that the open edge profile favourably impacts C_L and C_p for positive values of angle α.

The use of CFX software for analysis of airflow over wind turbine airfoil was shown to be appropriate. Such a way of studying flow conditions is cheaper, but nevertheless presents an experiment an essential tool for the validation of computations and understanding the dynamics of the phenomenon.

The improvement of numerically computed lift coefficients in the case of an open trailing edge airfoil may seem highly significant, but it is necessary to take into account that it is just a two-dimensional numerical computation, for which no kinetic energy necessary for flow through open trailing edge of the profile was incorporated. Thus, a possibility for further research of flow conditions is offered, taking account of three dimensions, a greater number of blades, the rotation of the rotor and the changing angle of attack across the blade into account.

It would be intriguing to see how that kind of blade would behave in a laboratory experiment, from which a more realistic picture and validation of the assumed hypothesis could be obtained.

References

[1]   **A. Hribernik**: *Obnovljivi viri energije*, Maribor: Založništvo Fakultete za strojništvo, 2010.

[2]   **M. Eberlinc, B. Širok and M. Hočevar**: *"Patented Hollow Blades of the Axial Fan with Trailing Edge Self-Induced Blowing"* Recent Patents on Mechanical Engineering, vol. 2, no. 1, pp. 1–7, 2009.

[3]   **J. D. Anderson**: *Fundamentals of aerodynamics*, 3rd ed., New York: McGraw-Hill, 2001.

[4]   **Aerospace engineering**: *"Aerospace engineering"* February 2013. [Online]. Available: http://aerospaceengineeringblog.com/bio-mimetic-drag-reduction-2/.

[5]   **M. Fike**: *Eksperimentalna in numerična raziskava tokovnih pojavov v aksialnem ventilatorju*, Maribor: Fakulteta za strojništvo, 2013.

[6]   **I. H. Abbott and A. E. Von Doenhoff**: *Theory of wing sections*, Canada: General Publishing Company, 1959.

[7]   **M. Eberlinc, B. Širok, M. Dular and M. Hočevar**: *"Modification of axial fan flow by trailing edge self-induced blowing"* Journal of Fluids Engineering, vol. 131, November 2009.

[8]   ANSYS, Help, 14.0 ed., 2011.

[9]   **T. Burton, N. Jenkins, S. David and E. Bossanyi**: *Wind energy handbook*, 2 ed., United Kingdom: John Wiley & Sons, Ltd., 2011.

[10]   **E. L. Houghton and P. W. Carpenter**: *Aerodynamics for engineering students*, 5 ed., Butterworth-Heineman, 2003.

[11]   **M. Malgaj**: *"Obnovljivi viri v EU in položaj Slovenije"* February 2013. [Online]. Available: http://www.zelenaslovenija.si/images/stories/pdf_dokumenti/Obnovljivi-viri-energije-v-Sloveniji.pdf.

[12]   **A. Predin**: *Vetrne turbine*, Maribor, 2011.

Nomenclature

(Symbols)	(Symbol meaning)
A	Area
A	axial force
C_L	lift coefficient
C_D	drag coefficient
c	chord length
D	drag force
F_x	axial force
L	lift force
l	characteristic length
M	Torque
$\dot{m}$	mass flow rate
N	normal force
P_{tot}	airstream power
P	Power
P_{maks}	maximum power
p_∞	upstream pressure
p	Pressure
R	resultant of aerodynamic forces
S	reference area
S_M	momentum sources
t	Time
u	tangential velocity
U	time averaged mixture velocity
v_∞	free stream velocity
α	angle of attack
η_{maks}	maximum coefficient
λ	tip speed ratio
ν	kinematic viscosity
ρ_∞	free stream air density
τ	shear stress; stress tensor

A SULPHUR HEXAFLUOROIDE GAS LEAKAGE DETECTION SYSTEM USING WIRELESS SENSOR NETWORKS

SISTEM ODKRIVANJA UHAJANJA PLINA ŽVEPLOVEGA HEKSAFLOURIDA Z UPORABO BREZŽIČNIH SENZORSKIH MREŽ

Damir Šoštarić[ℜ], Goran Horvat, Srete Nikolovski

Keywords: sulphur hexafluoride gas, SF_6, circuit breakers, gas leakage, WSN

Abstract

Most high-voltage (HV) transformer stations currently use sulphur hexafluoride (SF_6) gas as a dielectric to prevent arcing in circuit breakers. The excellent dielectric properties of SF_6 allow HV equipment to be constructed in only 10–20% of the volume/space of air insulation. Reductions of SF_6 gas density in circuit breakers cause failures in providing the required interrupter insulating properties and can lead to operational inefficiencies and safety hazards. SF_6 has a global warming potential 23,900 times that of CO_2; therefore, any leakages must be strictly monitored. The most fundamental measure against the uncontrolled emission of the SF_6 gas into the atmosphere is the constant monitoring and detection of its leakage in energy facilities. The methods for the SF_6 leakage detection should be extremely precise, while simultaneously having acceptable implementation costs. This paper presents a solution for an SF_6 gas monitoring system using Wireless Sensor Network (WSN) nodes. These nodes use multi-hop networking to transmit data to a base station connected to the other stations and the internet through a secure VPN (Virtual Private Network) connection. Using wireless sensing systems also significantly decreases installation time and reduces costs of materials and labour.

[ℜ] Corresponding author: Damir Šoštarić, MEng., Tel.: +385-31-224-600, Fax: +385-31-224-605, Mailing address: Kneza Trpimira 2B, 31000 Osijek, Croatia
E-mail address: damir.sostaric@etfos.hr

Povzetek

Večina visoko napetostnih transformatorskih postaj trenutno uporablja plin žveplov heksaflourid (SF6) kot dielektrik, ki preprečuje preboje v odklopnikih. Odlične dielektrične lastnosti plina SF6 dovoljujejo visokonapetostni opremi, da je konstruirana le z 10-20% prostornine zračne izolacije. Zmanjšanje gostote plina SF6 v odklopnikih povzroča napake v zagotavljanju zahtevanih izolacijskih lastnostih naprave in lahko vodi k operativni neučinkovitosti ter ogroža varnost. SF6 ima veliko večji vpliv na globalno segrevanja (23900-krat večji od CO2), zato mora biti kakršnokoli puščanje nadzorovano. Najosnovnejši ukrep pred nenadzorovanimi emisijami plina SF6 v ozračje je konstantno spremljanje in zaznavanje puščanja plina v energetskih objektih. Metode detektiranja puščanja plina SF6 morajo biti izredno natančne, istočasno morajo imeti tudi sprejemljive stroške izvedbe. Članek predstavlja rešitev za nadzor količine plina SF6 z uporabo vozlišč v brezžičnem senzorskem omrežju. Ta vozlišča uporabljajo omrežje z mrežno topologijo za prenos podatkov do bazne postaje, ki je povezana z ostalimi postajami. Prav tako uporabljajo internetno povezavo s pomočjo vzpostavljene VPN povezave (virtualno privatno omrežje), ki omogoča dostop do skupnega omrežja preko varne neposredne povezave. Uporaba brezžičnih senzorskih sistemov bistveno zmanjša čas montaže in stroške materiala ter dela.

1   INTRODUCTION

The key role of SF_6 gas in circuit breakers is to extinguish electrical arcs when contacts inside the circuit breaker are pulled apart. SF_6 has a global warming potential of 23,900 times that of CO_2 (compared over a hundred year period). SF_6 is also a highly stable gas, and its atmospheric lifetime is 3200 years. Therefore, working with SF_6 gas has to be strictly monitored. The most fundamental measure against the uncontrolled emission of the SF_6 gas into the atmosphere is the constant monitoring and detection of its leakage in energy facilities. The methods of leakage detection should be extremely precise (enabling the detection of extremely low concentrations of the SF_6), while simultaneously having acceptable implementation costs.

The downside associated with the installation of SF_6-insulated switchgear has been the lack of diagnostic equipment able to establish the integrity of the insulating gas, which is a necessity considering the severe and costly damage that can occur if the unit suffers an in-service failure. This problem can be overcome by utilizing wireless sensor technology for monitoring transformer stations and substations. This could produce significant benefits for power utility companies. The wireless sensor network (WSN) can be used for monitoring the condition of critical and expensive equipment in transformer substations, which has many advantages in comparison to existing monitoring systems. Every sensor node should be protected with a metallic cover due to the high-voltage environment. The nodes use multi-hop networking to transmit data to a base station, which also should be protected. The base station is connected to the other stations and the internet through a secure VPN connection. Depending on their specific application, sensor installation nodes may have an autonomous power supply (long lasting batteries, solar power with rechargeable batteries) or use the external power available at the transformer substation. Using wireless sensing systems also significantly decreases time and reduces the costs of materials and labour.

A WSN based on sensor nodes equipped with sensors for the detection of SF_6 gas can be the core of a state-of-the-art SF_6 monitoring and leakage detection system. Through the gateway,

----

the WSN is connected to the local area network (LAN) and to the internet (optional possibility). Therefore, the information obtained from the sensors can be available worldwide. Such an approach is more precise and less expensive in comparison to conventional wired methods. Moreover, it is more reliable, more flexible and easily extended.

The prototype WSN for SF_6 detection is based on Crossbow's MICAz wireless sensor nodes extended with SF_6 detectors. The standard for wireless communication between nodes is 2.4 GHz ZigBee (IEEE 802.15.4). The sensor network is connected to the local area network through the NB100 Stargate NetBridge gateway. Due to multiple points of SF_6 leakage detection, such a system is tolerant on failures of certain sensor nodes.

In the following section, the role of SF_6 gas in circuit breakers is described in detail. The environmental impact of SF_6 gas leakage is depicted in Section III, while proposed system for SF_6 gas leakage detection system is described in detail in Section IV. Section V gives the conclusion.

2   THE ROLE OF SF_6 IN CIRCUIT BREAKERS

In a transformer substation, a key element is the high voltage circuit-breaker (CB). Its role is to open and close the generator, transformer, and distribution transmission line terminals in order to protect electrical equipment against overload and short circuit currents. A prerequisite for the basic operation of a circuit breaker is excellent arc quenching for switching. This is realised using SF_6 gas.

SF_6 gas is used inside circuit breakers to extinguish the electrical arc when contacts inside the circuit breaker are pulled apart, thus enabling the electrical circuit to be broken. The excellent dielectric properties of SF_6 allow HV equipment to be constructed in only 10–20% of the volume/space compared to air insulation. Gas amounts can vary between a few to 300 kg SF_6 per gas compartment. SF_6 circuit breakers are closed pressure systems, which means that the SF_6 gas under pressure is closed in the tank, and its volume is replenished only periodically by manual connection to an external gas source. The equipment can only function properly if no or only minimal emissions of SF_6 exist; therefore, keeping the gas sealed is a basic issue. Reduction of SF_6 gas density in circuit breakers causes failure to provide required interrupter insulating properties and can lead to operational inefficiencies and significantly reduced safety.

The main causes of serious faults in CB, i.e. failures with interruptions to service, are identified as the operating mechanism failure and leakage of the insulating medium SF_6. This gas is increasingly used in the high-voltage electrical industry because it is an excellent dielectric, has an exceptionally strong electrical arc switching characteristic, and is chemically inert, non-toxic and non-flammable. At present, there is no known dielectric and breaking agent better than SF_6 gas, so there are no viable alternatives to it in the high-voltage electrical industry.

The use of SF_6 technology results in compact equipment with low material usage, high operational safety, minimized fire load and high availability. There is also a positive ecological balance because of lower energy losses compared to conventional AIS solutions (therefore, it contributes to CO_2 reduction).

----

3   ENVIRONMENTAL CONCERNS RELATED TO SF$_6$ GAS

The Kyoto Protocol designated SF$_6$ as a greenhouse gas (GHG) whose release to the atmosphere needs to be limited. The Global Warming Potential (GWP) of this gas is 23,900 greater than that of CO$_2$ 1, so it can contribute to the man-made greenhouse-effect, if it is released into the atmosphere. SF$_6$ is also highly stable gas, and its atmospheric lifetime is 3200 years. Consequently, awareness of the climatic effect of SF$_6$ became common after 1995, and since then the usage of SF$_6$ gas has been given increasing attention. Practical productions require correspondence with European Regulators' Group for Electricity and Gas, Smart Metering with a Focus on Electricity and Gas Regulation [1].

To the year 2002, it is estimated that SF$_6$ had contributed only 0.28% of total EU-15 greenhouse gas emissions (Figure 1), [2]. SF$_6$ emissions from electrical power equipment contribute less than 0.05% to the total European GHG effect, [2]. Because of high expected future rates for SF$_6$ use, significant efforts have been made in recent years to implement emission reduction measures dedicated especially to fluorinated gases. The level of emissions over the expected CB lifetime of 40 to 50 years depends on specific design elements of the equipment and the production process, but also on lifetime maintenance requirements, SF$_6$ handling equipment and procedures. From the mid-1990s onward, manufacturers and users active began reducing and controlling emissions. Many efforts are being made to reduce the emission of SF$_6$ to the lowest level possible during the life cycle of the circuit breaker, from the development phase, the manufacturing process, then during its service life, particularly during maintenance and at the end of life of the equipment.

Figure 1: *The rate of SF$_6$ in total EU-15 greenhouse gas emissions in 2002, [2]*
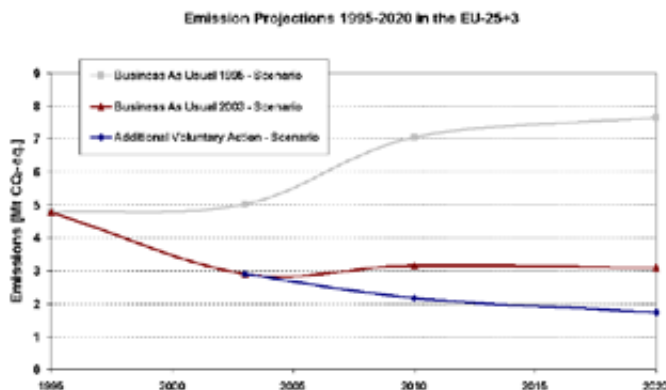
Figure 2: *Emission projections 1995-2020 for three Scenarios, [2]*

Owing to the continuous improvement of products (more compact, lower emission, low leakage rates during the lifetime of the equipment) in that period, leakage rates for new equipment are below 0.5% p.a. for closed pressure equipment. This made it possible to introduce the IEC 62271-1 standard in 2004, which states that maximal leakage can be 0.5%/p.a. However, a large number of older circuit breakers that were not produced according to such a standard remain; their condition has to be monitored.

Despite better characteristics of new circuit breakers, according to [2], SF_6 emissions were projected to rise after 2003 without further action by manufacturers and users due to strong bank growth. Therefore, further European & global realization of emission reduction is necessary.

Volunteer actions of manufacturers and users (utilities) of electrical high and medium voltage equipment in Europe realized a reduction of 40 % SF_6-emission from 4,8 Mt CO_2-eq in 1995 to 2.9 Mt CO_2-eq in 2003 (see Figure 2) by improved handling of SF_6 throughout the lifecycle of SF6-equipment including manufacture, use and end-of-life, despite a significant increase of the bank of SF6 in electrical equipment.

For the HV sector using SF_6-filled HV electrical equipment, there is neither a restriction nor any limitation to the use of SF_6 in electrical equipment above 1000 V. That is because SF_6 is characterized by excellent insulation and arc quenching with no equivalent at the moment. Efforts to find alternative fluids for SF_6 of the same functionality, but less overall environment impact have not been successful. However, there is a reduction of losses in the HV power network as an indirect effect of SF_6-insulated equipment, because one ton of installed SF_6 in HV applications would save 0.8 GWh per year, which also means a reduction CO_2 emissions. The EU-F-Gas-regulation intends to ensure that blue scenario from Figure 3 is met.

Figure 3: *SF₆ Breakers failures in Croatia/World*

Regarding the reliability data for Croatian power system components in 2004–2008 period, the circuit breakers have average frequency of failures f = 2.877 for 1/100 pieces a year. This is the highest value for frequency failures among all components. There is total of 830 breakers in HV transmission network in Croatia, among which are approximately about 400 SF_6 circuit breakers. Improving their reliability using WSN SF_6 leakage detector monitoring will have significant influence on overall reliability of the Croatian power system and in reducing electrical power outages to the consumer on the 110 kV voltage level.

4   WSN MONITORING SYSTEM FOR SF₆ LEAKAGE

Networks of sensors are widely used for monitoring and control applications. In a communication network, deployment of wires is expensive and can cause problems during normal operations and maintenance. Wireless sensor networks efficiently eliminate the need for wires, but also open many new application domains. Reliability and low-power consumption are the two key factors that determine the performance of a WSN. Collecting and delivering SF_6 gas sensor data over a wireless sensor network is a convenient way to automate older high voltage substations without requiring expensive and invasive retrofits. WSN technology could enable a wide spectrum of other functions at substations to be remotely monitored at a reasonable cost.

Leaks of SF_6 gas are rare, but effectively detecting and preventing them has clear benefits for the environment, as well as for improving system reliability and performance through reduced maintenance costs and the prevention of costly equipment failures. The utilization of wireless sensor technology for monitoring transformer stations and substations could produce significant benefits for power utility companies.

The sensor nodes use multi-hop networking to transmit data to a base station, which should also be protected. The base station is connected to the other stations and the intranet through

the secure VPN connection. Wireless sensors can be used for monitoring many different parameters. One example of potential usage is the monitoring of transformer surface temperatures or surface temperatures of the circuit breakers in order to detect anomalous or fault conditions. They can also be used for the detection of transformer bushing degradation by detecting phase differences between the obtained voltages. Wireless sensor nodes can also be equipped with mechanical, acoustic or chemical sensors for monitoring vibrations, acoustic discharge sensing and detecting certain chemicals in the air, such as fumes and other dangerous gases. Depending on their specific application, sensor nodes may have autonomous power supply (long-lasting batteries, solar power with rechargeable batteries) or use the external power available at the transformer substation. Using wireless sensing systems also significantly decreases installation time and reduces costs of materials and labour.

a)   b)
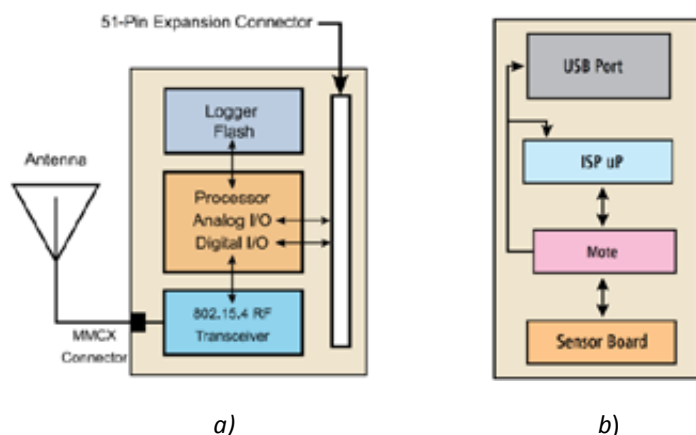
Figure 4: *a)WSN Block Diagram; b) Programmable Base Station*

The recently developed technology of wireless sensor networks has immense potential for the use in power transformer stations for SF_6 leakage detection. The nodes of a wireless sensor network include adequate sensors, a data processing unit, a wireless communication subsystem and the battery power unit. Such sensor nodes are low-power and low-cost devices capable of mutual wireless communication with the base station.

The prototype of wireless sensor network for SF_6 gas detection is based on Crossbow's MICAz wireless sensor nodes extended with the SF_6 sensors. The standard for wireless communication between nodes is 2.4 GHz ZigBee (IEEE 802.15.4). The maximum packet size supported by 802.15.4 is 128 bytes, and the maximum raw data rate is 250kbps. Power consumption of the proposed system is as follows: Processor- 8mA under load, 15μA in sleep; Radio- 27111.4 transmit, l0mA receive, lμA sleep; expected lifetime is 1 year on AA batteries; Operating system- TinyOS.
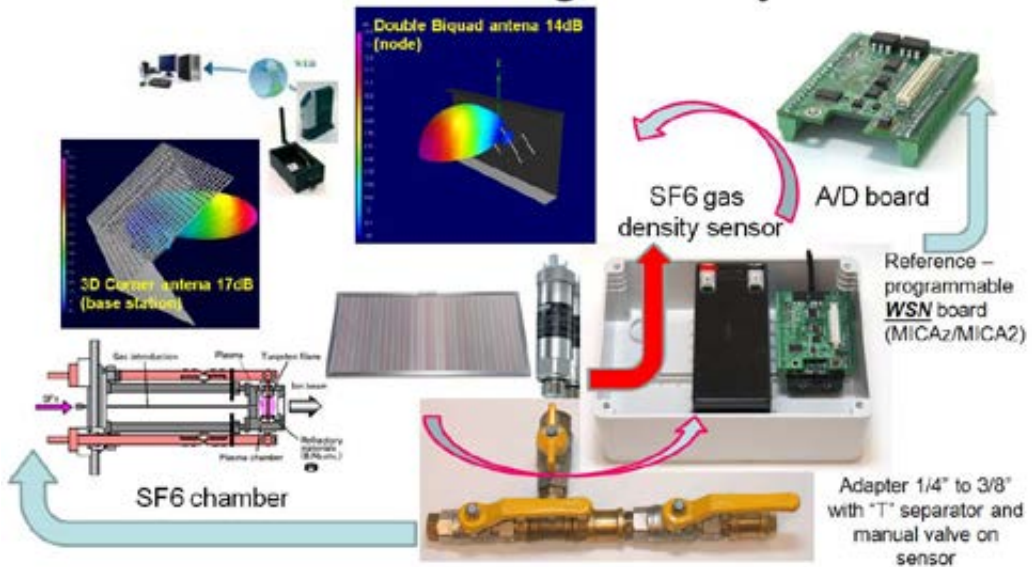
Figure 5: *Monitoring the leakage of SF_6 gas from the chamber, [3]*

The sensor network is connected to the local area network through the *NB100 Stargate NetBridge* gateway. Due to multiple points of SF_6 leakage detection, such a system is tolerant of failures of certain sensor nodes.

The development of the custom-designed sensor application is enabled through *Crossbow's MoteWorks* software platform, which allows programming sensor nodes via the programmer or via a remote computer over the supervisory. A local database allows *XServe* (internal application) to store and process sensor network information. *XServe* effectively bridges these different realms through the support of standard XML APIs.

Figure 5 shows the remote monitoring system realized using a wireless sensor node extended with an MDA300 data acquisition board. A mechanical T-divider is envisaged for combining the monitoring system and circuit breaker chamber, and also for chamber replenishment. The mechanical valve setup ensures the protection of the sensor during the chamber replenishment and provides a sensor replacement with minimal SF_6 leakage. Since the sensor requires an additional power supply, the system includes a solar panel connected to a battery and control circuitry. Besides the analogue input for data about SF_6 density (adc0 channel), other analogue channels (adc1 and adc2) serve for the battery voltage measurement and charging. The calculation of the Rs (shunt resistance) gives the electric current signal termination on MDA300

----

board. The linearization of input measures was performed with the polynomial integration in firmware. Such linearization is an element for future work. Standard antennas provide a range of approximately 70 meters, while setup of double-bi-quad and 3D corner antennas provided larger coverage.

The principle of the sensor is based on the two chambers, of which one is the reference and the other the measurement chamber, [5]. The difference in the resonant frequencies in the chambers (vacuum and SF_6) is manifested as a current (I [mA]) signal through the DC–DC converter. The current size is the main measurement that defines the density and the pressure in the chamber.

The development of custom sensor applications is enabled through Crossbow's *MoteWorks* software platform, which is specifically optimized for low-power battery-operated networks and provides support for sensor devices, server gateways and user interface. The server gateway is based on middleware (*XServe*) for connecting wireless sensor networks to enterprise information and management systems. *XServe* is the glue layer that connects the wireless sensor network to enterprise or industrial networks through standard XML. Due to the low-power and memory footprint requirements in wireless sensor networks, communication is streamlined through message formats and network protocols.
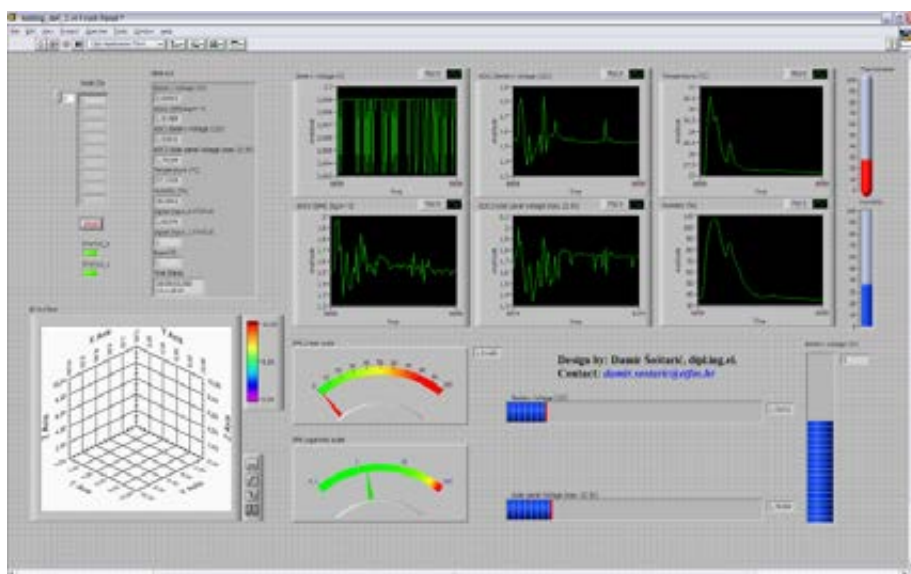
Figure 6: *An example of user interface for SF_6 monitoring based on MICAz with data acquisition board MDA 300 and National Instruments LabView 2011, [6]*

This differs from the IP protocols used in IT back-end systems or existing industrial networks. XServe effectively bridges these different worlds through the support of standard XML APIs. A local database allows XServe to store and process sensor and network information. Integration with back-end monitoring, control and management systems delivers the full value of wireless sensor networks to enterprises and makes the connection of the physical world with the internet a reality.

The user interface for the Crossbow platform can be *MoteView* or a third party product like *LabView* (Figure 6) functioning as a client application for remote analysis, monitoring, management and configuration of the sensor network. Standardized interfaces should allow easy system upgrading.

5   CONCLUSION

Wireless sensor networks can be used for monitoring the condition of critical and expensive equipment in transformer substations, providing many advantages in comparison to existing monitoring systems. These advantages include lower installation costs and utilization of the distributed processing capabilities of the wireless sensor nodes to provide smarter sensing mechanisms, [8]. Certainly, the great advantage of wireless sensing technology is the elimination of the risks of on-site data collection from the high-voltage substation. Wireless sensor nodes can be equipped with different types of sensors and deployed throughout the station to monitor different critical parameters. Every sensor node should be protected with a metallic cover due to the high-voltage environment. Existing solutions based only on pressure measurement are not sufficiently precise, [7]. There are approximately 400 SF_6 circuit breakers in the HV transmission network in Croatia. Improving their reliability using WSN SF_6 leakage detector monitoring will have significant influence on overall reliability of the Croatian power system and on reducing un-supplied electrical energy to the consumer on 110 kV voltage level. In reference to the future system functionality, the system could be extended to additional sensors in WSN, for example accelerometer/gyroscope in three axes, ultrasound, vibration sensors (in terms of strain gauges) etc.

References

[1]   European Regulators' Group for Electricity and Gas, *Smart Metering with a Focus on Electricity Regulation*, Document E07-RMF-04-03, 31 October 2007.

[2]   **S. Wartmann, J. Harnisch:** *Reduction of SF6 emissions from high and medium voltage electrical equipment in Europe*, Final Report to CAPIEL, Project No.: dm70047.2 Ecofys, 28 June 2005.

[3]   CEA Project No. 485T1049 *On-line Condition Monitoring of Substation Power Equipment - Utility Needs*

[4]   **Hiroyuki Yusa,** et.al., 2007, *Architecture of Information Network System for Substation Facility Maintenance*, Joint technical meeting on power engineering and power systems engineering, IEE Japan, PE07-70, PSE-07-85, pp. 25-30

[5]   Trafag High Voltage SF6 Gas Density Sensor. Model 8774.50.1104.52.26.X0.; http://www.trafag.com/data-sheet/H72507.pdf

[6]   **Dirman Hanafi, Mohamed Najib Ribuan, Ignatius Agung Wibowo, Hairulazwan Hashim, Muhamad Izzuddin Ismail.:** *Simulation of Substation Integrated Monitoring System using LabView*, Global Journal of Technology & Optimization, Volume 2, 2011.

[7]   Avistar solution:

http://www.epa.gov/electricpower-sf6/documents/conf06_willard.pdf

----

[8]   **G. Horvat, D. Šoštarić, Z. Balkić:** *Cost-effective Ethernet Communication for Low Cost Microcontroller Architecture*, 1-8., IJECES 2012.

THE VELENJE COAL MINE'S SPATIAL MONITORING OF SURFACE AND STRUCTURE MOVEMENTS

SPREMLJANJE PREMIKOV POVRŠINE IN OBJEKTOV NA OBMOČJU PREMOGOVNIKA VELENJE

Drago Potočnik, Janez Rošer[ℜ], Milivoj Vulić

Abstract

The Velenje Coal Mine's (VCM) system of surface observation is complex and can be classified as an extended geodetic monitoring system. In addition to the standard geodetic techniques (triangulation, trilateration, levelling, GNSS), it also includes more modern methods such as aerophotogrammetry, terrestrial laser scanning and an automatic Real-Time GNSS Deformation Monitoring System. By using the Real-Time GNSS Deformation Monitoring System, we are able to monitor not only the potential impact of mining on the power plant facilities but also the impact of the newly constructed power generating facility, Unit 6, and the combined effects on existing facilities. With an extended geodetic monitoring system, the surface movements and deformations on over 300 measurement points in the Šalek Valley are observed. Furthermore, with sonar measurements, we are determining the Šalek lakes' bottom surface and performing observations of structure movements and deformations. The extended VCM geodetic monitoring system is constantly being expanded and upgraded with new measurements and the latest equipment.

[ℜ] Corresponding author: Janez Rošer, PhD, Tel.: +386 3 899 6496, Fax: +386 3 899 6635, Mailing address: PV Invest d.o.o., Koroška cesta 62b, SI-3320 Velenje
E-mail address: janez.roser@pvinvest.si

Povzetek

Premogovnik Velenje d.d. je za potrebe spremljanja in zagotavljanja varnosti na območju pridobivalnega prostora in širše vzpostavil takšen sistem opazovanja površja, da ga lahko klasificiramo kot razširjen geodetski monitoring sistem. Ta zajema poleg standardnih geodetskih tehnik (triangulacija, trilateracija, nivelman, GNSS) tudi modernejše metode, med katere sodijo aerofotogrametrija, terestrično lasersko skeniranje in samodejni GNSS sistem za spremljanje pomikov in deformacij v realnem času. S slednjim ne samo da preventivno spremljamo potencialni vpliv rudarjenja na objekte Termoelektrarne Šoštanj (TEŠ), ampak tudi vpliv novogradnje Bloka 6 TEŠ ter kombinirane vplive na obstoječe objekte. Z razširjenim geodetskim monitoring sistemom spremljamo premike in deformacije površine na preko 300 merskih točkah v Šaleški dolini, izvajamo sonarske meritve za določitev dna šaleških jezer ter premike in deformacije objektov (npr. Klasirnica PV in TEŠ). Razširjen geodetski monitoring Premogovnika Velenje nenehno razširjamo z novimi meritvami ter ga nadgrajujemo z najsodobnejšo opremo.

1   INTRODUCTION

The Velenje Coal Mine (Premogovnik Velenje d.d.), the largest Slovenian coal mine, with an annual production of four million tonnes of coal, sends nearly all of the extracted coal to the Šoštanj Thermal Power Plant (Termoelektrarna Šoštanj) for the production of electricity. The technology of coal extraction is carried out with the Velenje Mining Method [1], resulting in subsidence of the overlying strata and the formation of surface depressions. Figure 1 shows the Šalek Valley with the mine roadways of the Velenje Coal Mine in black. Since the security of significant energy installations, such as thermal power plants and coal mines, and their impact on the environment are vital for the efficient operation and associated good public opinion, movements of the surface and deformations of structures have been monitored under the auspices of the technical services of the Velenje Coal Mine.

Figure 1: *A broader area of the Velenje Coal Mine showing the mine roadways (black) and points of observation networks on the surface (red).*

Monitoring the movement of the surface covers measurements of observation networks, dams between lakes and the bottoms of lakes; moreover, monitoring of nearby industrial and residential buildings is also carried out. Today, it can be said that the system for monitoring the surface and installations, and for further forecasting movements of the terrain with the help of computer models can be classified as an expanded geodetic monitoring system.

2 METHODS OF MONITORING MOVEMENTS AND DEFORMATIONS

As a part of monitoring the movements and deformations on a wider area of the Velenje Coal Mine, we carry out measurements on the surface and individual buildings (Figure 2).

Surface movement monitoring
- triangulation, trilateration
- geometric levelling
- GNSS measurements
- aerophotogrammetry
- bathymetry

Building structure movement monitoring
- triangulation, trilateration
- geometric levelling
- continuous GNSS measurements
- terrestrial laser scanner
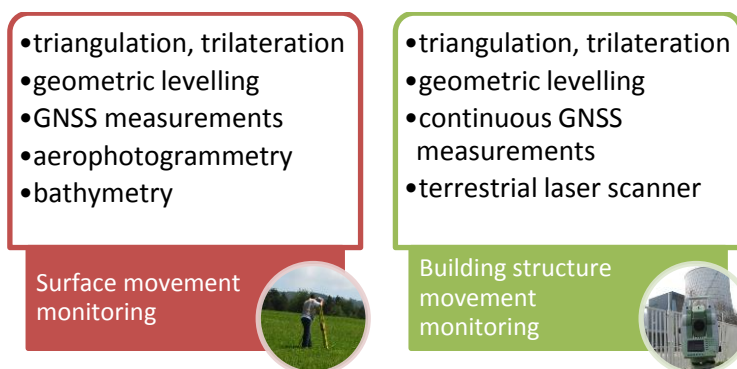
Figure 2: The methods of monitoring movements and deformations on the area of The Velenje Coal Mine.

2.1 Monitoring of the surface

2.1.1 Monitoring of the surface

The impact of excavation on the surface is reflected in the changes in the terrain with the formation of depressions on the surface shortly after starting excavations, reaching 90% of its final value about three months after the end of excavations. Since many excavation panels are active at the same time in the Velenje Coal Mine and the excavation of one begins immediately after the excavation of another ends, it is difficult to discuss the impact of one particular excavation panel on the surface. With the measurements of the observed points on the surface, we monitor the development of the movements due to more excavation panels on a particular area on the surface. Because we carry out the measurements of the field movements in the spring, we discuss the impact of the excavations that have been under excavation the year before the measurements.

We monitor over 300 observation points on the surface on the wider area of the Velenje Coal Mine, which we group into observation networks (Table 1). To determine the coordinates of the base points of each observation network, which are an integral part of the main network of the Velenje Coal Mine, the so-called Small Geodynamic Network of the Velenje Coal Mine, we carry

----

out measurements with the GNSS (Global Navigation Satellite System) method of surveying. We carry out the observation of points of most of the observation networks with a classic terrestrial method of measurement, whose results are three-dimensional coordinates (Y, X, H) in the National Gauss-Krüger coordinate system. For a more accurate determination of the heights of the observation points of certain networks, we also use the method of geometric levelling. The measurements of the observation networks are generally carried out at least once a year; in specific cases, they are carried out more often, as much as many times per month (Table 1).

Table 1: The observation networks of the Velenje Coal Mine with the number of measured points, type and frequency of measurement.

Name of network	*Number of points*	*Type of measurement*	*Frequency [annually]*
MGM PV	18	GNSS	1
Glavna PV	145	T + N	1
Pesje	25	T + N	1
Škale	21	T + N	1
Gaberke	29	GNSS	1
Ravne	12	GNSS	1
Videčnik	25	T + N	12
Turn	9	T + N	4
Pocajt	6	T + N	12
Kompan	4	T + N	4
Blatnik	2	N	6
TEŠ	6	T + N	12
NOP II	7	GNSS	4
NOP II	12	T + N	12
Legend:			
T – terrestrial measurement method N – method of geometric levelling			

2.1.2 Aerophotogrammetry

Within the pilot project, we also carried out aerophotogrammetry of the surface directly over the excavation panel G2C in the Preloge mine (Figure 3). Aerophotogrammetry is a measurement technique for recording the earth's surface from the air and, on the basis of the acquired imagery, the elaboration of plans and making of a digital elevation model of the terrain, [2]. The excavation of the G2C panel started on 16 May 2010 and finished on 31 January 2011. The excavation was horizontal; the average height of the excavation panel was 5.2m [3]. Aerophotogrammetry was carried out in three periods: in April and September of 2010, and in April of 2011. The photogrammetric measurement was made with an automatic correlation of

----

the heights in a raster of 5×5 m. The basis for geo-locating the photogrammetric measurements was approximately 10 points that were marked on the field and measured with the Differential GNSS method. Apart from that, a larger number of points were also measured on the field, which served for improving the photogrammetric measurements and controlling the results.

Figure 3: *The locations of the excavation panel G2C in the Preloge mine of The Velenje Coal Mine.*

2.1.3 Bathymetric measurement of lakes

In the Šalek Valley, there are three subsidence lakes, which are a result of coal extraction (Figure 1). Measuring the lakes is intended for observation and tracking the impact of the excavations to the surface and the transformation of the terrain; it is carried out once a year. In PV Invest d.o.o., Reason NaviSound 110 sonar has been used for measuring the depths since 2010, as it enables connection to a computer and GNSS device; the results of the measurements are points with given Y, X, Z coordinates and the depth. The procedure for measuring lakes is as follows: the lakes are measured in a square net with the sonar and the GNSS determination of the location in real time (RTK method); the size of a cell is approximately 25 metres; measurements are made every 5 metres (Y, X, H, depth). At the same time, measurements of the temperature of the water at different depths are performed. What follows is the processing of the depth data, where the impact of the water temperature on the speed of sound transmission in the water is taken into consideration. Furthermore, a model of the lakebed is made from the corrected measurements. Based on models of the lakebed from each year, subsidence areas under the lakes can be seen.

2.1   Monitoring building structures

The subsidence of the surface consequently endanger building structures on the impacted area of excavations, with hairline cracks first appearing, followed by moderate structural damage, and possibly finishing with a collapse. Within the boundaries of the extraction area, there is a

----

small number of building on which the monitoring of movements and deformations is carried out if necessary. The decision to do so depends on both the expected movements of the surface near the building, and the actual state, which is obtained via continuous measurements of the observation networks.

In PV Invest d.o.o., movements and deformations of buildings are monitored using the classic method of land surveying, but also with the use of terrestrial laser scanning (TLS), and with the advanced automatic continuous GNSS monitoring system for displacements and deformations in real-time, which consist of the most advanced measuring instruments and software specially designed for deformation monitoring.

2.2.1 Monitoring building structures with the methods of classic and GNSS measurement

Monitoring of the movement of buildings is done with the methods of classic land survey, i.e. with terrestrial surveying method and the method of geometric levelling. Relative GNSS surveying methods with post-processing of observations that provide maximum precision in position determination may also be used. Such measurements are carried out on buildings that are located near areas where movement has already detected, or, in the vicinity of expected movement (Figure 4).

Figure 4: *Monitoring the movements on a building with: the method of geometric levelling (left), the static GNSS measurement (middle), the use of a 3D terrestrial laser scanner (right).*

On a stable area in the vicinity of the building, a basic network is set up. The most suitable method is to carry out the measurements with the terrestrial method through individual points of the basic network. When this cannot be done, it must be ensured that the 'free-station' locations for observing buildings through linear and angular measurements are connected to at least three points from the appropriate network. The measurements are conducted in many sets, based on which the coordinates of the 'free-station' locations are individually assigned each time. From the 'free-station' locations, the characteristic points that are to be built into the building, also in many sets, are then observed.

As part of optimizing the transport routes in the Coal Mine Velenje, a new 505-meter deep shaft for the transport of coal to the surface is being made. Cave surveying services, in the construction of the shaft NOP II, cover, in the first phase, setting up the basic initial observation network of the shaft, through which the movement and deformation areas of the shaft and the

----

shaft itself during its construction are monitored. Regardless of the building to be monitored, the starting observation network must be designed so that it is possible to carry out control measurements of its stability, and that it is possible to determine the size of the movement of each observed point in the network at any time of the measurements, [4]. Points of the initial observation network are placed around the construction site of the shaft so that the visibility is provided between them (Figure 5). The location of pillar points has been predetermined on the basis of the position of buildings on the construction site and the photo of the broader state around the building (landfill). The final locations of points are thus determined on the basis of the control visibility between points on the field after the finished construction of the main buildings on the construction site of the NOP II shaft.
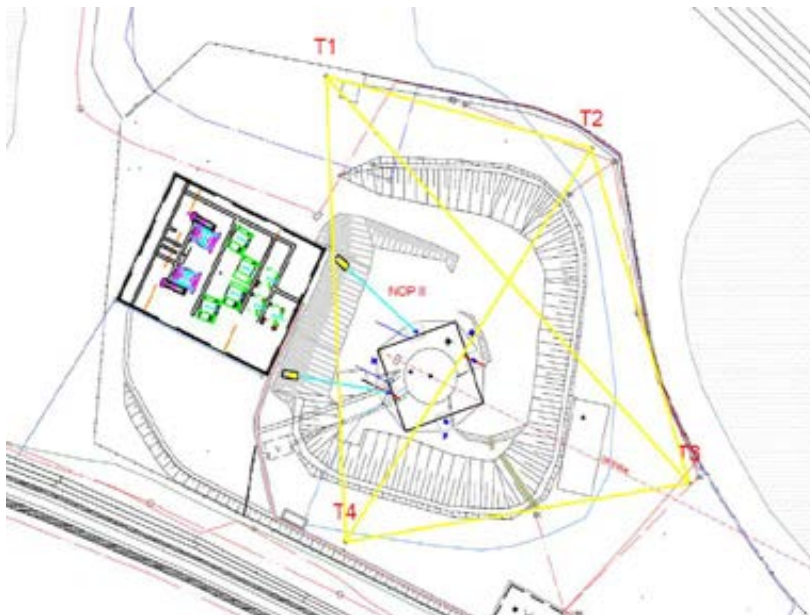
Figure 5: *The situation in the area of the NOP II shaft with the observation pillars – points of the initial NOP II network.*

The basic local observation network of the NOP II shaft is made up of four control points (T1, T2, T3 and T4), which are located in the NOP II shaft area (Figure 5) and three reference points, which are part of the MGM PV. Observations in the initial observation network are carried out, [4]:

- Once a month terrestrially in at least three sets with the electronic Leica TPS 1201+ tachymeter. This means that the horizontal and vertical movements in the network are determined with the electronic tachymeter by measuring the horizontal direction, vertical angles and inclined lengths. Furthermore, the vertical movements are determined with a more precise geometric levelling. Angular observations are carried out via the method of sets. In this way, the internal stability and non-deformability of the basic initial network NOP II is controlled.
- Once every three months, the initial observation network is attached to the basic PV grid. These measurements are carried out with a static GNSS measurement with the

----

use of Leica GPS1200+ GPS receivers. In this way, the movements of the basic initial network of the NOP II shaft and the stability of the external network are determined.

2.2.2 Monitoring building structures using the terrestrial laser scanner (TLS)

Scanning with a terrestrial laser scanner enables the creation of a highly precise surface network of an area or building, which is extremely important for the perception of spatial changes between instances of measurement. The company PV Invest d.o.o., in co-operation with the Faculty of Natural Sciences and Engineering of the University of Ljubljana, has conducted a scanning of the sorting plant building of the Velenje Coal Mine in two periods separated by nine months, [5]. The measurement was carried out with the Leica Scanstation 3D terrestrial laser scanner (Figure 4, right), while the processing and modelling were carried out with the Cyclone and AutoCad programs. The final interpretation was made in the program MS Excel. In total, 9,326,790 points were captured and, after filtering clutter and eliminating the irrelevant points, there were 4,986,600 points used at the end. The registration and geo-referencing was based on five connection points whose coordinates were determined with classic (TPS) measurements.

2.2.3 Automatic continuous GNSS system

As part of the preparatory work and hereinafter the construction of TEŠ Unit 6, PV Invest d.o.o. conducts measurements of stability of the existing building, as well as calculations of movement and the preciseness of the movement. For this purpose, a measurement network of the automatic uninterrupted GNSS monitoring has been established, which consists of three GNSS observation points (GMX N, GMX S in GMX E) that are located at the periphery of the top of the cooling tower of Unit 4, two observation points with a tilt sensor (NIVEL n and NIVEL s) that are located above the ground at the periphery of the top of the cooling tower of Unit 4, a reference (stable) GNSS point (GRS O) is placed in the facility of the pumping station of TEŠ on the Paka River, next to it is also a point-with-a-tilt sensor (GRS o) (Figure 6). All points are directly linked to the central computer where observations of all the sensors are collected. The central computer can be accessed remotely via the internet, enabling examination of the measurements whenever and wherever desired. A detailed schematic is shown in [6]. The software is configured for automatic conversion of three basis vectors: the GRSO-GMXN, GRSO-GMXS and GRSO-GMXE. Automatic parameters that are post-processed by GNSS and a 15° angle are chosen. For the purpose of further analysis of achievable precision in dependence of the length of measurement time, products were created every: 10 min, 30 min, 1 h (for experimental purposes) and every 3 h, 6 h, 12 h, 24 h. To determine the movements, 24-hour intervals of measurement were selected, as the expected movements are slow and the highest accuracy was achieved (order of mm).

Figure 6: *The position of the measuring points of the automatic uninterrupted GNSS monitoring in TEŠ.*

3 RESULTS

3.1 Monitoring of the surface

3.1.1 Observation networks

Based on the processed point measurements of observation networks from different periods of measurement, the movements are calculated. The result of the horizontal and vertical movements of the observed points is made into a table and a graphical display according to individual years; the maps of the isolines of the movements are also plotted (Figure 7).
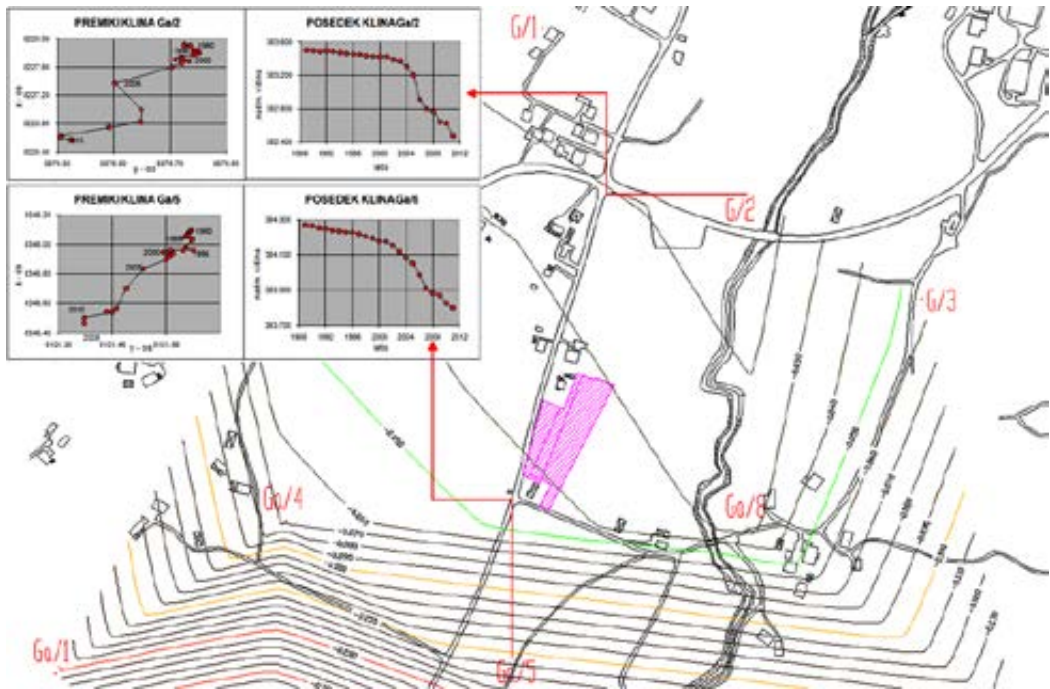
Figure 7: A map of the vertical movement isolines made based on the results of measurements in two periods of the observed points, and a graphical display of the individual points' movements.

3.1.2 Aerophotogrammetry

The final results of the calculated subsidence based on the aerophotogrammetry from measurements of three periods are shown in Figure 8. The results reflect the expected maximum settlements in the area of the excavation panel, which are decreasing in the directions away from the excavation panel. The results are consistent with the anticipated chronology of the terrain subsidence; the terrain subsidence, which refer to the changes in April 2010–September 2010 (the excavation is active for about five months), are smaller than the terrain changes in the period of April 2010–April 2011 (the excavation is complete). Detailed results are shown in [7].
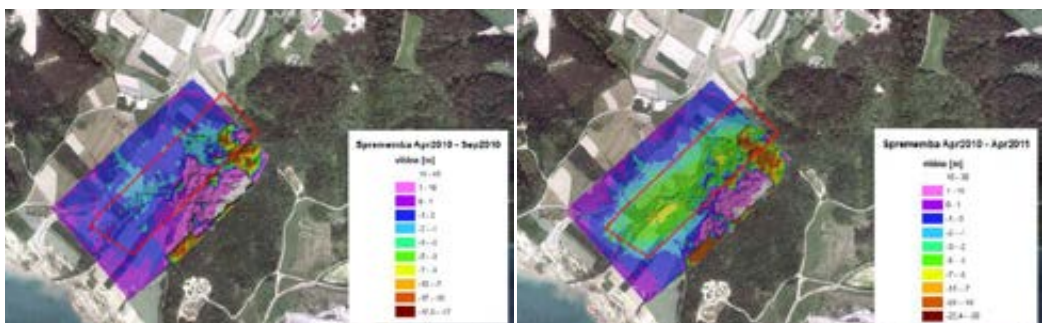
Figure 8: The results of changes in calculated terrain subsidence on the basis of aerophotogrammetry: April 2010–September 2010 (left) and April 2010–April 2011 (right).

3.1.3 Bathymetric measurement of lakes

The depth measurement data of the Šalek lakes is essential in monitoring the subsidence area that is filled with water. A comparison of results measurements with previous measurements provides insight into the changes that have occurred within one or more years, [8]. Figure 9 shows a bathymetric map of the Velenje Lake (left) and a 3D model of the lakebed (right). The maximum depth is 63.22 m, the average depth is 23.42 m, the volume is 33,634,785 m³, the surface area is 1,436,183 m² and the altitude is 366.538 m.
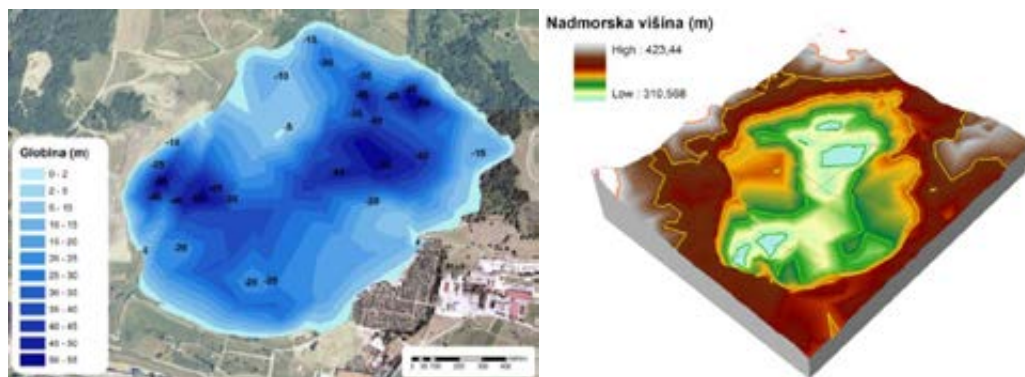
Figure 9: A bathymetric map (left) and a 3D model of the Velenje Lake lakebed (right).

3.2   Monitoring building structures

3.2.1 Monitoring building structures with the classic measurement method

The example on Figure 10 shows a facility on which cracks are beginning to appear. In the period from May 2008 onward, the facility has been measured with the height method of geometric levelling through built-in benchmarks. These are included in conducting measurements of the horizontal network by using the method of sets.
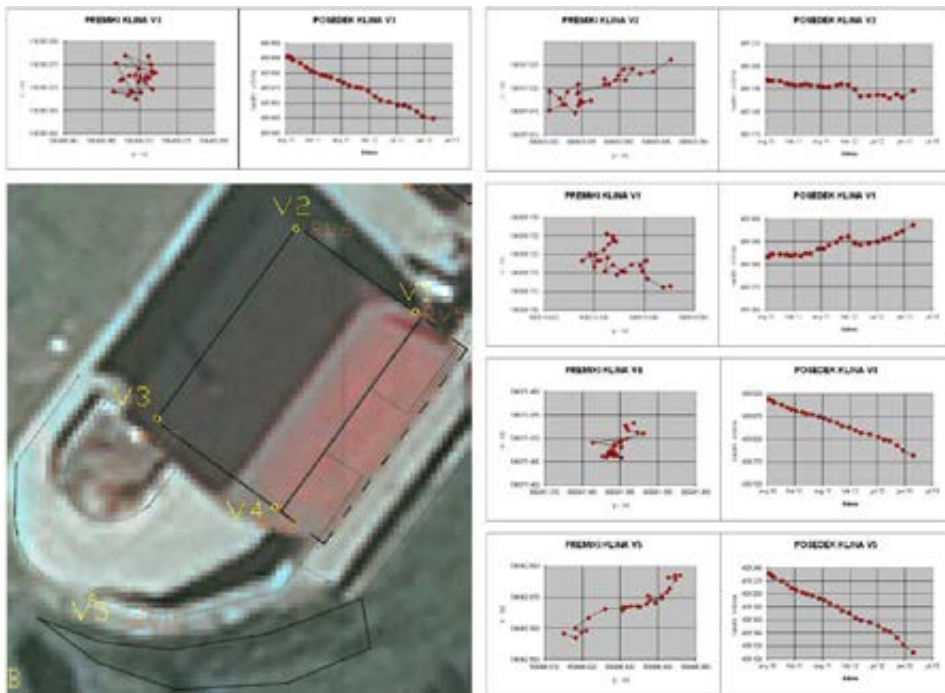
Figure 10: *A graphical display of the results of a monitoring of the movements of the facility over the course of several years.*

The observation network measurements of the NOP II shaft began in December 2012; to date, six measurements have been made using the terrestrial measurement method and the method of geometric levelling, as well as two GNSS period measurements. It is clear from the results of measurements that the movements in the shaft area are minimal (Figure 11), [4].
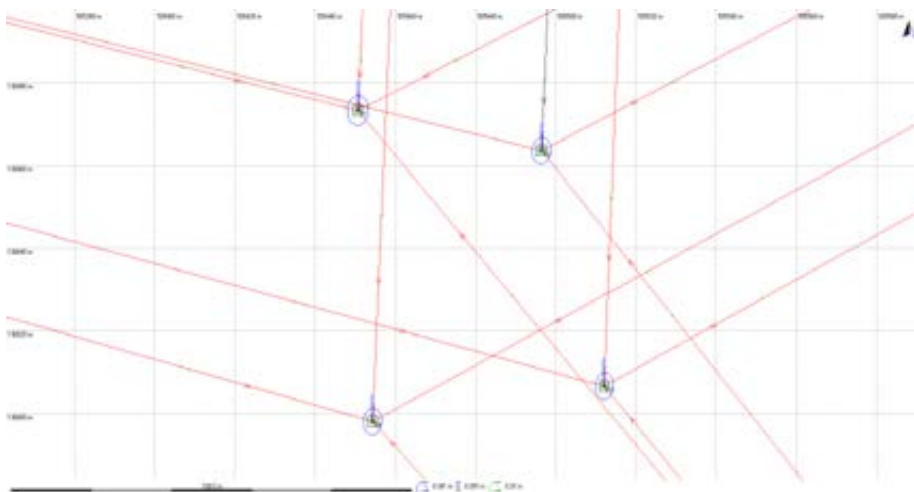
Figure 11: *A graphical result of the GNSS processed points of the base observation network of the NOP II shaft.*

3.2.2 Monitoring the building structures using TLS

Measurements on PV sorting plant building have taken place mostly in order to confirm whether the method is suitable for the observation of such movements. Scannograms of the building in two measurement periods from the processed measurements were obtained, and with the calculation of deviations between pairs of the same points of individual measurements the movements have been calculated (Figure 12). Based on the achieved accuracy of 0.4 mm, which provides detection of movement ≥ 1.3 mm with a 99% probability, it follows that the observed points on the sorting plant building have moved up to 4 cm, [5]. According the results, the necessary procedures for ensuring safety of the building and its reinforcement were predicted. With the process of modelling carried out, the computational processing of data and the results obtained, the 3D terrestrial laser scanning with the scanner proved to be suitable for solving such tasks.
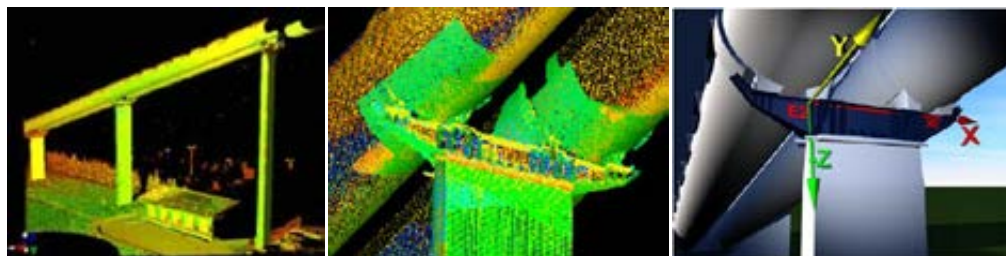
Figure 12: *A scannogram of the observed building (left), a display of a certain detail (middle) and the final model of the building with the coordinate axes shown (right).*

3.2.3 Automatic continuous GNSS system

For the period from 25 September 2010 to 30 April 2013, an analysis was made of the data obtained and the results of observations. Figure 13 (left) shows a coordinate deviation of the observed point GMX E in the direction of axis X (yellow), Y (red) and Z (blue). Of course, on the basis of only a few measurements, conclusions cannot be made on the movement of the observed point, as the accuracy of individual measurements depends on several factors, such as variable meteorological conditions, satellite constellations, mistakes during capturing the data in the 'on the fly' mode. Consequently, the regression functions in real time has also been calculated, which provides a more realistic picture of the change of position of the observed point, and constitutes an effective method for determining whether this is indeed movement or not (Figure 13 right). In this case, the-so called monotonic piecewise cubic interpolation for the regression function was used [9], [10].
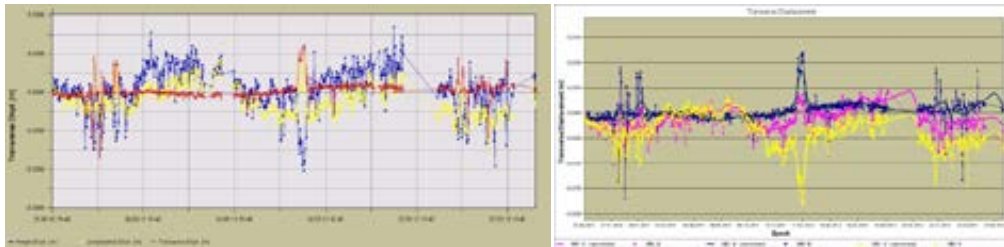
Figure 13: *The coordinate deviation of the point GMX E; X yellow, Y red, Z blue (left), and the coordinate deviation of all three points together with the calculated regression curve; GMX N blue, GMX E pink, GMX S yellow (right).*

The analysis of the accuracy evaluation of the observed points GMX N, GMX E, and GMX S is calculated on the basis of more than 700 twenty-four hour intervals. In case of long-term observations, the accuracy of the measurements within 0.5 mm. Based on that, it can be concluded that the chosen interval of 24 hours is suitable for monitoring a selected building for which no sudden changes are expected, [11].

4   DISCUSSION

The consequences of the mining industry in the Šalek Valley can be seen on the surface as a development of subsidence, which filled with water and led to the formation of three Šalek lakes. With the intent of controlling the events taking place in the extraction area of Velenje Coal Mine, surface movements and vital facilities are monitored consistently. The movement observation system consists of observation networks, which have been used for monitoring over 300 surface points in recent decades. Before 1990, network measurements were conducted only by a combination of triangulation and trilateration for the plane network and a geometric levelling for the height network. However, with the development of satellite technologies and the GNSS system, at the Velenje Coal Mine an observation network on the basis of GNSS measurements was established. Such points represent a much better basis for establishing the coordinates of the mining observation networks' main points, which we then use for measurements of the observation networks. However, surface movements have a negative effect on all neighbouring facilities. By monitoring these movements and the deformation of close industrial and residential facilities, we are able to provide safe working and living conditions. Moreover, we are able to calculate position changes of surface points and facilities in any given time frame using these observations.

As part of monitoring the surface, annual measurements of the Šalek lakes are conducted. These measurements serve the purpose of observing and monitoring the influence of mining on the surface and the reshaping of the terrain. The first measurements of the Velenje lake date back to 1960, but since 1975, regular measurements have been performed on all three lakes.

The extensive geodetic monitoring of the Velenje Coal Mine is constantly being expanded with new measurements and upgraded with the latest equipment. Among the more current techniques, terrestrial laser scanning for the observation of buildings must be mentioned, which was tested by monitoring the movements of the PV sorting plant facility, as well as the automatic GNSS monitoring system, which enables a graphic display of data in real time, which can also be accessed over the internet. Surface monitoring, in contrast, was performed with

----

aerophotogrammetry, which proved only partially useful, as forest-covered areas produce inaccurate results. An alternative to this is the LIDAR (Light Detection and Ranging) method, which enables the distinction between the laser beam reflections from actual terrain and those from trees. However, compared to the aforementioned aerophotogrammetry, the price of this method is less favourable.

The main advantages of extended VCM monitoring system, though, are its well-developed methodology, its usage capabilities, the fact that it has been extensively tested, and the manner of assessing the results. The monitoring feature also provides data about the system's accuracy, correct technical procedures, and efficient measures when confronted with known or unknown phenomena.

References

[1] **M. Medved, L. Golob.:** *Sustainable development of Velenje Mining Method and its global use*, 4th Balkanmine Congress, Slovenia, Ljubljana, 2011.

[2] **K. Kraus:** *Photogrammetry – Geometry from Images and Laser Scans*, 2nd Edition, Walter de Gruyter, Berlin, 2007.

[3] *Rudarski projekt - PID, Priprava in odkopavanje odkopne plošče G2/C*, Premogovnik Velenje, Velenje, 2010.

[4] **D. Potočnik**: *Raziskave, modifikacije in vpeljevanje nove metodologije jamomerskih dejavnosti pri izgradnji vertikalnih jaškov (v rokopisu)*, 2013.

[5] **G. Novaković**: *Primerjava terminskih izmer s 3D laserskim skenerjem na objektu Klasirnica Velenje* – diplomsko delo, 2009.

[6] **D. Potočnik, J. Rošer, A. Lamot, M. Vulić**: *Real-Time Deformation and Movement monitoring using GNSS in the Šoštanj Thermal Power Plant*, Balkanmine 2011, 543–550 Ljubljana.

[7] **A. Bilc, J. Rošer**: *Tehnologija izvedbe aerosnemanja vplivnega območja odkopa G2C – Gaberke od letenja, zajemanja in obdelave podatkov, do rezultatov*. Zbornik posvetovanja Društva tehničnih vodij površinskega odkopavanja, 2011.

[8] **J. Rošer, D. Potočnik**: *Aktivnosti pri spremljanju stanja šaleških jezer in deponije premoga*, Rudar – razvojni dosežki Skupine Premogovnik Velenje, 2011.

[9] Leica Geosystems, 2008. *Help Manual GeoMoS*, version 4.0.

[10] **F.N. Fritsch, R.E. Carlson:** *Monotone Piecewise Cubic Interpolation*, SIAM J. Numer. Anal. Vol 17, No. 2, April 1980.

[11] **J. Rošer, I. Ristović, M. Vulić**: *Applicability of Continuous Real-Time Monitoring Systems in Safety Assurance of Significant Structures*, Strojarstvo 52 (4) 449–458 (2010).

IMPACT OF STAINLESS STEEL GUIDE TUBES ON THE REACTIVITY PARAMETERS OF THE NPP KRŠKO CORE

VPLIV VODIL IZ NERJAVNEGA JEKLA NA REAKTIVNOSTNE PARAMETRE SREDICE NUKLEARNE ELEKTRARNE KRŠKO

Marjan Kromar[ℜ], Bojan Kurinčič

Abstract

PWR fuel assemblies with Zircaloy-based guide tubes experience some level of bowing during nuclear plant operation. Severe bowing could present difficulties impacting plant performance. Bowing could be mitigated with a reintroduction of stainless steel guide tubes. The impact of such tubes on the reactivity parameters of NPP Krško fuel is investigated in this paper. An analysis has shown that the stainless steel guide tubes lower critical boron concentration by about 140 ppm. To compensate this effect and retain the cycle length, fuel enrichment should be increased by 0.2%. The combined changes result in a 100 ppm higher boron concentration at the beginning of the fuel cycle and increase isothermal temperature coefficient by approximately 1 pcm/K compared to the Zircaloy-based fuel. Core power distributions and power peaking factors remain almost the same. Increased thermal neutron shielding in the stainless steel guide tubes lowers control rods worth up to 3% in relative terms. Analysis has shown that the replacement of the Zircaloy with stainless steel as a guide tube material could become a viable solution to mitigate fuel bowing problems.

[ℜ] Corresponding author: Marjan Kromar, PhD., Tel.: +386 1 588 5292, Fax: +386 1 588 5377, Mailing address: Jožef Stefan Institute, Reactor Physics Department, Jamova cesta 39, 1000 Ljubljana, Slovenia.
E-mail address: marjan.kromar@ijs.si

Povzetek

Vsak gorivni elementi v tlačnovodnem reaktorju z vodili iz cirkalojeve zlitine občuti večje ali manjše zvijanje. Znatno zvijanje lahko povzroči motnje v obratovanju in vpliva na učinkovitost proizvodnje. S ponovno uvedbo vodil iz nerjavnega jekla lahko zvijanje omejimo. V prispevku je predstavljen vpliv menjave materiala vodil na reaktivnostne parametre goriva v Nuklearni elektrarni Krško. Analiza je pokazala, da vodila iz nerjavnega jekla zmanjšajo kritično borovo koncentracijo za 140 ppm. Za kompenzacijo tega efekta in ohranitev dolžine gorivnega cikla je potrebno povečati obogatitev goriva za 0.2 %. Obe spremembi posledično povzročita dvig kritične borove koncentracije na začetku cikla za 100 ppm in s tem dvigneta izotermični temperaturni koeficient za približno 1 pcm/K glede na izhodiščno gorivo z vodili iz cirkaloja. Porazdelitve moči v sredici in konični faktorji ostanejo praktično nespremenjeni. Povečano nevtronsko ščitenje v vodilih iz nerjavnega jekla zniža vrednost kontrolnih palic relativno za 3 %. Analiza je pokazala, da vpeljava vodil iz nerjavnega jekla predstavlja uporabno rešitev za omilitev problemov zvijanja goriva.

1   INTRODUCTION

Guide tubes form the main structural component of the fuel assembly (FA). In conjunction with the grids and with the end nozzles, they act as the main load-carrying parts of the FA. They serve as a support structure and a guide path for the control elements such as control rods, neutron sources and in-core instrumentation. The structural behavior of the FA is affected by changes in the length of the guide tubes resulting from elastic deformation, irradiation growth, hydrogen pickup, oxide layer formation induced creep and creep under the axial load. Variations of guide tube and fuel rod elongation rate across the FA tend to put the FA structure in tension, which could result in the assembly bowing.

Extreme FA bow can lead to:

- ➢ increased times for control rod insertion or even incomplete rod insertion,
- ➢ excessive water gaps between fuel assemblies affecting the local power,
- ➢ increased probability of the grid-to-rod fretting wear,
- ➢ handling difficulties impacting nuclear plant performance, or even grid damage during reshuffling.

Originally, the PWR guide tubes were made of stainless steel (for example, Westinghouse Standard 14×14 fuel W1414W and 15× 5 fuel W1515W). PWR fuel assemblies with stainless steel (SS) guide tubes did not show any significant length change and only very little bow. In the second half of the 1970s, the material for the guide tubes was changed to Zircaloy, to reduce neutron absorption and improve fuel economy. PWR fuel assemblies with Zircaloy-based guide tubes experience some bowing during the operation. Severe bow in several power plants has been reported since 1990. Recently, some utilities decided to mitigate the fuel assembly bow problem with the reintroduction of SS guide tubes into the fairly new fuel assembly design.

In this paper, the impact of stainless steel guide tubes on the reactivity parameters of the NPP Krško fuel is investigated.

----

2   METHODS

NPP Krško is a two-loop Westinghouse PWR plant with a gross electrical output of 730 MW. The core consists of 121 fuel assemblies. Each assembly has 235 fuel rods arranged in a 16×16 array. The remaining 21 positions contain guide tubes and are intended for control rods, neutron source and in-core instrumentation. In Figure 1, the radial cross section of the NPP Krško fuel is presented. Fuel rods are represented with red; 21 guide tube channels are clearly visible.
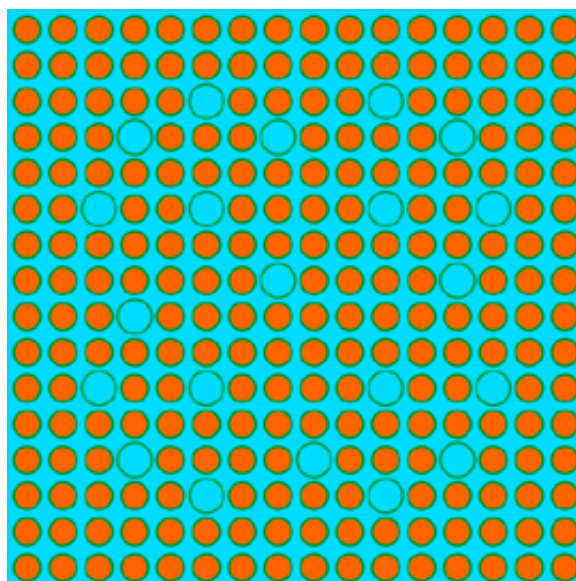
Figure 1: *Radial cross section of the NPP Krško fuel assembly*

Two computer codes were used in the analysis:

> ➤ Serpent, [1],
> ➤ CORD-2, [2,3].

Serpent is a three-dimensional continuous-energy Monte Carlo reactor physics burnup calculation code, developed at VTT Technical Research Centre of Finland. It uses a continuous energy neutron cross section library in an ACE format based on the ENDF/B-VII.0 evaluated nuclear data library, [4]. The code is specialized for two-dimensional lattice physics calculations, but the universe-based geometry description also allows the modeling of complicated three-dimensional geometries. Detailed geometrical modeling of the NPP Krško fuel assembly in the code enables accurate determination of the neutron multiplication factor.

The CORD-2 system, developed by the Reactor Physics Department of the Jožef Stefan Institute, is intended for core design calculations of PWRs. The main goal in assembling the computational tools was to provide a non-commercial package that could be used for simple fast calculations (such as those frequently required for fuel management) as well as for accurate calculations (for example, core design after refueling). The CORD-2 system enables

----

determination of the core reactivity and power distribution. The package has been validated for the nuclear design calculations of PWR cores and has been used for the verification of the NPP Krško reload cores since 1990. A 69-group neutron cross-section library based on the ENDFB-VII.0 neutron data files has been used.

3   RESULTS AND DISCUSSION

3.1   Fuel assembly calculation

The CORD-2 system has not been validated for fuel assemblies with SS guide tubes. Although the influence on neutron transport is not expected to be very large, since the fuel rods and overall dimensions remain the same, it is prudent to validate the model. To accomplish this task, a typical fuel assembly at approximately average Hot Full Power (HFP) conditions has been calculated in the radial and axial infinite geometry. The assumed state point thermal-hydraulic variables were: fuel temperature 900 K, cladding temperature 620 K, coolant pressure and temperature 15.5 Mpa and 580 K, boron concentration 500 ppm. The dimensions reflect thermal expansion at full power operation. SS-304 material composition was assumed for guide tubes. Fuel assembly burnout from 0 to 60000 MWd/tU has been simulated with Serpent and CORD-2.

Stainless steel is a stronger neutron absorber than Zircaloy. The introduction of SS guide tubes therefore reduces assembly reactivity. A reactivity decrease of the FA enriched to 4.75% during fuel burnout is presented in Figure 2. A slight dissipation of the Serpent results is caused by the statistical nature of the Monte Carlo method. In the Serpent run, 1000 generations of 20,000 neutrons have been taken into account. The statistical 1 σ error in all runs was around 10 pcm. One burnup calculation took around 20 hours using 24 Intel Xeon 2.67 GHz processors. An equivalent CORD-2 calculation was accomplished in less than two minutes using a single-processor desktop computer with a 2.1 GHz clock rate.

The comparison on Figure 2 shows good agreement between both codes for burnups up to 30,000 MWd/tU. For larger burnups, Serpent predicts smaller impact of the SS guide tubes. It seems that some neutron spectral effect influencing fuel isotopic composition has not been appropriately taken into account in the CORD-2 calculation. However, it should be noted that differences are occurring in a high burnup Fas, which in the reactor core are much less important than more reactive fuel with smaller burnup. In addition, typical average FAs burnup in the NPP Krško core is in the range from 15,000 MWd/tU at the beginning of fuel cycle to around 35,000 MWd/tU at the end of cycle. In this burnup range, the agreement between both codes is good. Nevertheless, it should be expected that CORD-2 calculations slightly overestimate the impact of the SS guide tube, but the calculations are suitable for the evaluation having in mind bounding nature of results.

If the utility wants to operate the plant with the same cycle length, enrichment of the fuel should be increased to compensate the reactivity drop caused by the introduction of the SS tubes. Enrichment of the FAs exhibiting the same k_∞ is shown in Figure 3: 4.75% enrichment of the standard FA with Zircaloy guide tubes is presented with horizontal line for illustrative purposes. The same trend as in Figure 2 can be observed. CORD-2 predicts a need for slightly higher enrichments at higher burnups. Nevertheless, it can be estimated that additional enrichment of 0.15% to 0.2% would be required to compensate the SS effect. Since in reality

----

FAs enrichment varies from cycle to cycle and the boron concentration is changing during the core burnout, more adequate value can be determined only with calculation of the entire reactor core.
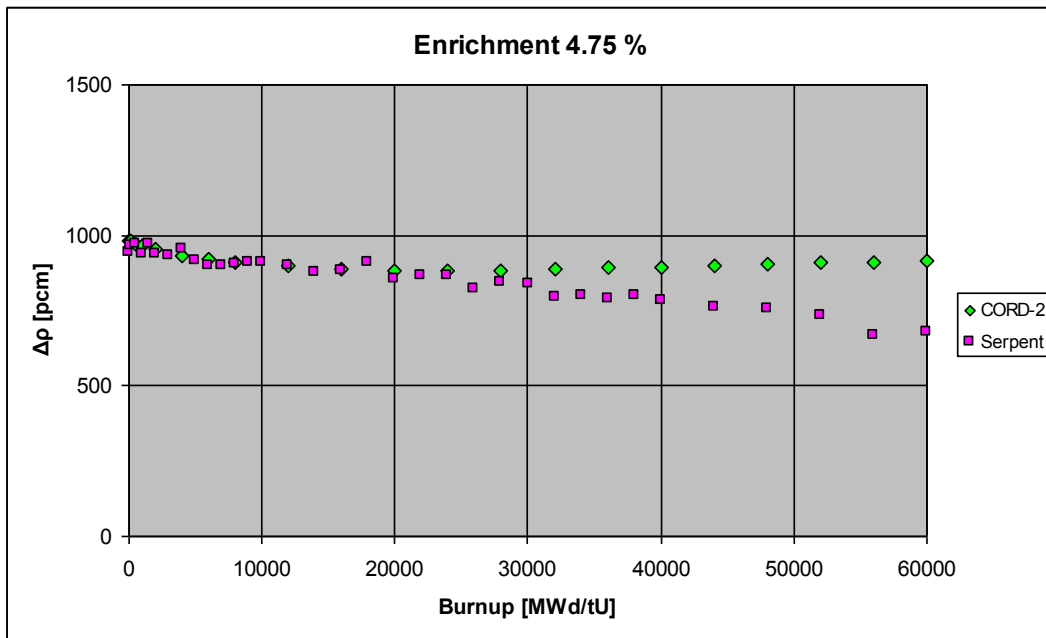
Figure 2: *Reactivity decrease caused by stainless steel guide tubes*
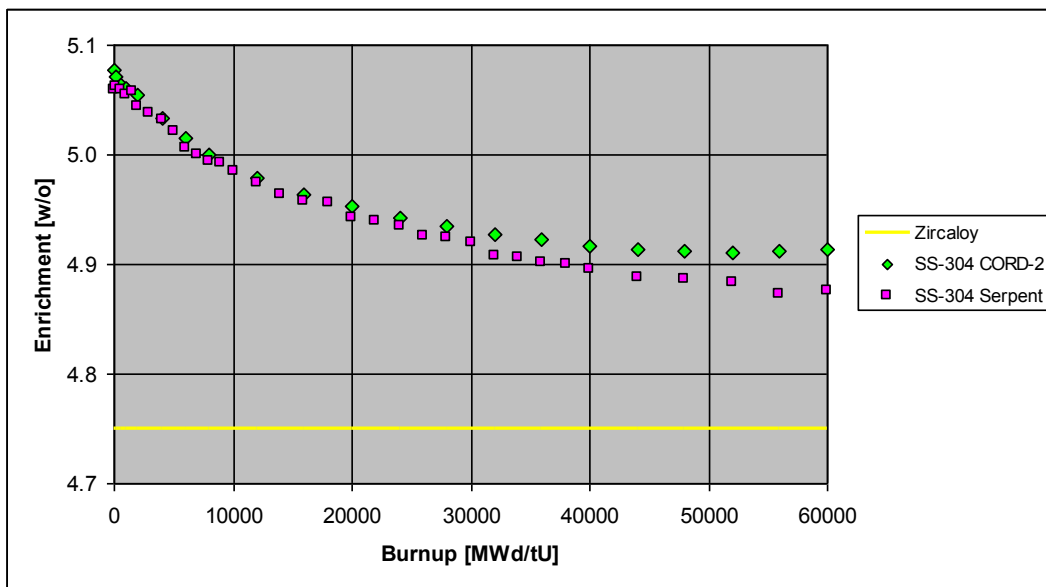
Figure 3: *Fuel assembly enrichment to yield an equivalent reactivity*

3.2   Core calculation

A typical 18-month NPP Krško fuel cycle has been investigated. Critical boron concentration at HFP conditions as a function of cycle burnup is presented in Figure 4. SS guide tubes lower boron concentration by about 140 ppm. That would shorten the fuel cycle by approximately 1500 MWd/tU or 37 days of full power operation. To compensate lower fuel reactivity, enrichment has to be increased to match the end of the cycle boron concentration. An enrichment increase of 0.2% was needed to match the fuel with Zircaloy guide tubes. Since the SS and enrichment effects are homogeneously distributed across the core, power distribution changes are small (less than 1%). Power peaking factors remain almost the same.
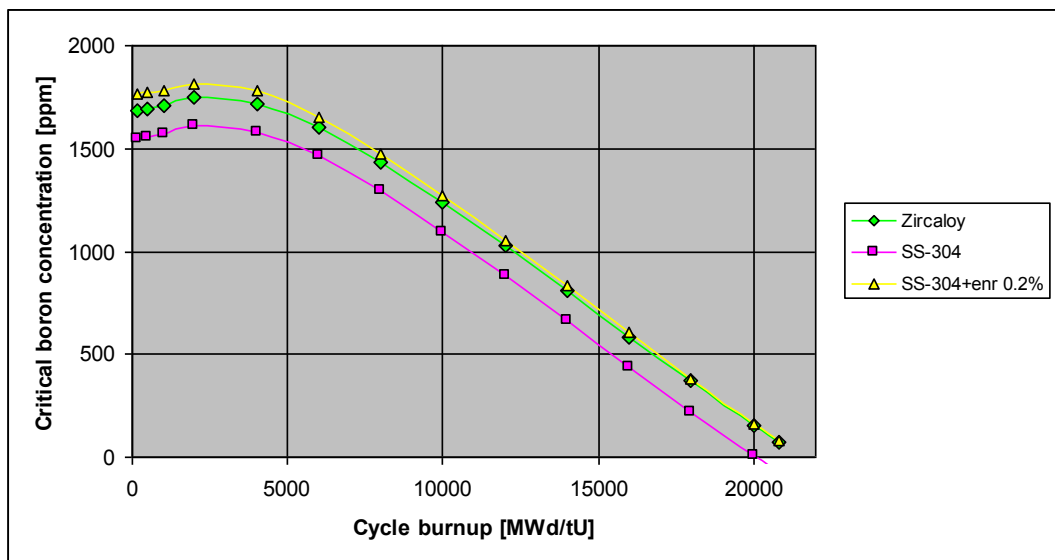
Figure 4: *Critical boron concentration versus cycle burnup at HFP, all rods out, equilibrium Xenon conditions*

Different boron concentrations induce different moderator and consequently isothermal temperature coefficients. This is especially important at the beginning of the fuel cycle with high boron concentration and high moderator temperature coefficient. The moderator coefficient is limited by the power plant technical specifications and shall be negative at all operational conditions. The isothermal coefficient is presented in Table 1. In the 'SS-304' case, the isothermal coefficient is lower, while in the 'SS-304 + 0.2% enrichment' case, the coefficient is 0.94 pcm/k higher.

The worth of the control rods is also presented in Table 1. In the case of SS guide tubes, the rods' worth is little lower. This is understandable, since the SS guide tubes shield thermal neutrons to reach the absorber rods more than Zircaloy tubes do. The effect is stronger at higher boron concentrations, since the rods physically drive out borated water from guide tubes.

Table 1: Isothermal temperature coefficient and rods worth

	Zircaloy	SS-304		SS-304 + 0.2% enrichment	
	Value	Value	Difference	Value	Difference
Isothermal temperature coefficient [pcm/k]	-5.20	-6.82	-1.62	-4.26	0.94
Bank D worth [pcm]	609	603	-6	599	-10
Bank C worth [pcm]	1044	1031	-13	1012	-32
Bank B worth [pcm]	988	973	-15	960	-28
Bank A worth [pcm]	958	948	-10	930	-28
Banks SA+SB worth [pcm]	2669	2636	-33	2590	-79
All banks worth [pcm]	6268	6191	-77	6091	-177

4   CONCLUSION

The impact of the stainless steel guide tubes on the reactivity parameters of the NPP Krško fuel is investigated. Stainless steel guide tubes lower the critical boron concentration by about 140 ppm. To compensate this effect, fuel enrichment should be increased by 0.2%. The combined effect results in the same end of the cycle boron concentration, while the boron concentration at the beginning of the cycle is around 100 ppm higher. The higher boron concentration consequently increases the isothermal temperature coefficient by around 1 pcm/K. Core power distribution and power peaking factors remain almost the same. Increased thermal neutron shielding in the stainless steel guide tubes lowers control rod worth by up to 3% in relative terms. The impact of the stainless steel guide tubes on the most important reactivity parameters is small. Their use is a viable solution to mitigate fuel bowing problems.

References

[1]   **J. Leppänen:** *PSG2 / Serpent – a Continuous-energy Monte Carlo Reactor Physics Burnup Calculation Code*, VTT Technical Research Centre of Finland, November 6, 2009.

[2]   **M. Kromar, A. Trkov:** *Nuclear Design Calculations of the NPP Krško core,* Journal of Energy Technology, Volume 2, Issue 4, 2009, pp. 41–50.

[3]   **A. Trkov, M. Ravnik:** *CORD-2 Package for PWR Nuclear Core Design Calculations,* Proceedings of the International Conference on Reactor Physics and Reactor computations, Tel-Aviv, 23–26. Jan. 1994, Beer-Sheva, Ben-Gurion University of the Negev Press, (1994).

----

[4]   **NEA Data Bank**: *ZZ SERPENT117-ACELIB, Continuous-energy X-sec lib., radioactive decay, fission yield data for SERPENT in ACE,* NEA-1854/01, http://www.oecd-nea.org/tools/abstract/detail/NEA-1854/.

AUTHOR INSTRUCTIONS (MAIN TITLE)

SLOVENIAN TITLE

Authors, Corresponding author[ℜ]

Key words: (Up to 10 keywords)

Abstract

Abstract should be up to 500 words long, with no pictures, photos, equations, tables, only text.

Povzetek

(In Slovenian language)

Submission of Manuscripts: All manuscripts must be submitted in English by e-mail to the editorial office at jet@uni-mb.si to ensure fast processing. Instructions for authors are also available online at http://www.fe.um.si/en/jet.html.

Preparation of manuscripts: Manuscripts must be typed in English in prescribed journal form (Word editor). A Word template is available at the Journal Home page.

A title page consists of the main title in the English and Slovenian languages; the author(s) name(s) as well as the address, affiliation, E-mail address, telephone and fax numbers of author(s). Corresponding author must be indicated.

Main title: should be centred and written with capital letters (ARIAL **bold** 18 pt), in first paragraph in English language, in second paragraph in Slovenian language.

Key words: A list of 3 up to 6 key words is essential for indexing purposes. (CALIBRI 10pt)

Abstract: Abstract should be up to 500 words long, with no pictures, photos, equations, tables, - text only.

Povzetek: - Abstract in Slovenian language.

[ℜ] Corresponding author and other authors: Title, Name and Surname, Tel.: +XXX x xxx xxx, Fax: +XXX x xxx xxx, Mailing address: xxxxxxxxxxxxxxxxxxxxxxxxxxxxxxxx, E-mail address: email@xxx.xx

----

<u>Main text</u> should be structured logically in chapters, sections and sub-sections. Type of letters is Calibri, 10pt, full justified.

<u>Units and abbreviations:</u> Required are SI units. Abbreviations must be given in text when firstl mentioned.

<u>Proofreading:</u> The proof will be send by e-mail to the corresponding author, who is required to make their proof corrections on a print-out of the article in pdf format. The corresponding author is responsible to introduce corrections of data in the paper. The Editors are not responsible for damage or loss of manuscripts submitted. Contributors are advised to keep copies of their manuscript, illustrations and all other materials.

The statements, opinions and data contained in this publication are solely those of the individual authors and not of the publisher and the Editors. Neither the publisher nor the Editors can accept any legal responsibility for errors that could appear during the process.

Chapter examples:

1   MAIN CHAPTER

(Arial bold, 12pt, after paragraph 6pt space)

1.1   Section

(Arial bold, 11pt, after paragraph 6pt space)

1.1.1 Sub-section

(Arial bold, 10pt, after paragraph 6pt space)

Example of Equation (lined 2 cm from left margin, equation number in normal brackets (section.equation number), lined right margin, paragraph space 6pt before in after line):

$$c = \sqrt{a^2 + b^2} \tag{1.1}$$

Tables should have a legend that includes the title of the table at the top of the table. Each table should be cited in the text.

Table legend example:

Table 1: *Name of the table (centred, on top of the table)*

Figures and images should be labelled sequentially numbered (Arabic numbers) and cited in the text – Fig.1 or Figure 1. The legend should be below the image, picture, photo or drawing.

Figure legend example:

Figure 1: *Name of the figure (centred, on bottom of image, photo, or drawing)*

References

[1]   **Name. Surname:** *Title,* Publisher, p.p., Year of Publication

Example of reference-1 citation: In text, Predin, [1], text continue. **(Reference number order!)**